A Visualization Study of Mixture Preparation Mechanisms for Port Fuel Injected Spark Ignition Engines

by

Vincent S. Costanzo

B.S. Mathematics
B.M.E. Mechanical Engineering
Villanova University, 2001

Submitted to the Department of Mechanical Engineering
in Partial Fulfillment of the Requirements for the Degree of

MASTER OF SCIENCE IN MECHANICAL ENGINEERING
AT THE
MASSACHUSETTS INSTITUTE OF TECHNOLOGY

JUNE 2004

Signature of Author: _____
Department of Mechanical Engineering
May 7, 2004

Certified by: _____
John B. Heywood
Professor of Mechanical Engineering
Thesis Supervisor

Accepted by: _____
Ain A. Sonin
Chairman, Departmental Graduate Committee

DISCLAIMER NOTICE

The accompanying media item for this thesis is available in the MIT Libraries or Institute Archives.

Thank you.

A Visualization Study of Mixture Preparation Mechanisms for Port Fuel Injected Spark Ignition Engines

by

Vincent S. Costanzo

B.S. Mathematics
B.M.E. Mechanical Engineering
Villanova University, 2001

Submitted to the Department of Mechanical Engineering
in Partial Fulfillment of the Requirements for the Degree of

MASTER OF SCIENCE IN MECHANICAL ENGINEERING
AT THE
MASSACHUSETTS INSTITUTE OF TECHNOLOGY

JUNE 2004

ABSTRACT

An experimental study was carried out that examined qualitatively the mixture preparation process in port fuel injected spark ignition engines. The primary variables in this study were intake valve lift, intake valve timing, injector spray quality, and injection timing. A special visualization engine was used to enable high-speed video of the fuel-air mixture flowing through the intake valve, as well as the wetting of the intake valve and head in the combustion chamber. Additionally, video was taken from within the intake port using a borescope to examine liquid fuel distribution in the port. Finally, a simulation study was carried out in order to understand how the various combinations of intake valve lifts and timings affect the flow velocity through the valve gap to aid in the interpretation of the videos.

The net result of the study was the construction of an "event diagram" for each experimental condition that identifies and explains the sequence of events and interactions affecting the liquid fuel. Six mechanisms that transport liquid fuel into the combustion chamber and five that affect liquid fuel within the combustion chamber were identified.

Thesis Supervisor: John Heywood
Title: Professor of Mechanical Engineering

Acknowledgements

My time at MIT has been made memorable by the people that I have gotten to know here, especially those in the Sloan Lab. I especially value the friendships of Jenny Topinka, Jeremy Llaniguez, and my camping buddies – Brian Hallgren, Alexis Rozantes, and Tiffany Groode. Brian and Alexis, you've been the big brother and big sister I never had. And Tiffany, you've been a very special friend and have taught me so much about so many things. I will forever cherish all of the "good times."

I would like to thank my advisor Prof. John Heywood for his guidance and truly remarkable insight into what mattered and what was only "second order." It never ceases to amaze me how problems I struggled with for weeks would suddenly become solved (or discovered to not be a problem at all) after a brief conversation with him.

The experimental setup would not have been possible without the help of numerous faculty and staff throughout the institute. Foremost, I would like to thank Prof. Wai Cheng for his electronics and troubleshooting assistance. I would also like to thank Thane DeWitt and Raymond Phan for their daily assistance in the lab, Jim Bales and Tony Caloggero in the Edgerton Center for their help with the high-speed video setup, Gerry Wentworth and Mark Belanger in the LMP machine shop for their assistance machining the rocker arms, and Prof. George Barbastathis for his discussion regarding the lighting challenges my setup posed.

The members of the Engine and Fuels Research Consortium have been extremely helpful in providing guidance and support. In particular, I want to thank Ron Herrin, Bob Lofthouse, Rick Davis, and Gerry Clark at General Motors for providing the camshafts and related assistance, Carilee Cole and Len Shebert at Delphi for providing the fuel injectors, Mike Pozar at Ford for his discussions and data regarding production variable valve control systems, and finally Mike Shelby and Brad VanDerWege (former caretakers of the square piston engine) at Ford for their help related to the test cell operation and maintenance.

This work would not have been possible without the funding provided by the Department of Defense and the Air Force Office of Scientific Research through a National Defense Science and Engineering Graduate Fellowship. Their support is gratefully acknowledged.

Finally, I want to thank all of my family and friends at home for their support. For their ability to remind me of life away from MIT and for just being a friend, I want to especially thank my grandparents and my friends Steve and Rob. Most importantly, though, I want to thank my parents. They have been a constant source of encouragement and support and without them the past several years would have been much more difficult. Thank you, Mom and Dad, for everything.

TABLE OF CONTENTS

LIST OF FIGURES

LIST OF TABLES

1 Background

1.1 The mixture preparation problem

A fundamental problem in gasoline-fueled spark ignition (SI) engines is that the fuel is stored in liquid form but must vaporize in order to burn in the combustion chamber. Currently, the most common method of preparing the fuel-air mixture in SI engines is port fuel injection. With port fuel injection, fuel is sprayed from an atomizing injector that is targeted toward the backside of the intake valve(s), and to a lesser extent the intake port walls. The intake valve is the hottest surface in the intake system, and thus evaporation of any liquid fuel films occurs most readily from it.

The main advantage of port fuel injection is that it has a better transient response relative to other approaches in which the fuel-air mixture is prepared further upstream in the intake system, such as throttle-body injection or carburetion [1]. However, this also means there is less time available for liquid fuel to evaporate, which can be problematic since the fuel is deposited directly outside the combustion chamber.

As a result, when the intake valve and port walls are not sufficiently warm it can be necessary to enrich heavily to ensure that enough fuel is delivered in vapor form to produce a combustible mixture [2]. Thus, with port fuel injection under cold (i.e. ambient) engine conditions, a significant amount of liquid fuel can be present in the intake port.

The intake valve and port wall temperatures affect the extent of fuel film evaporation. Any liquid fuel that remains will undergo physical processes that may or may not improve fuel vaporization. These processes are primarily affected by the nature of the flow through the intake valve. For this reason, the valve gap velocity history will be an important means of characterizing and understanding these mixture preparation mechanisms.

1.2 Hydrocarbon (HC) emissions regulations

Figure 1.1 shows the U.S. Federal Test Procedure regulations for passenger vehicle emissions of non-methane organic gases (hydrocarbons excluding methane) against the first year the regulation was implemented [3]. It should be noted that it is not mandatory for manufacturers to meet the regulations the first year they are implemented. The general trend is a factor of ten reduction in allowable hydrocarbons every fifteen years.

For the 1997 regulations, sixty to eighty percent of the total allowable tailpipe hydrocarbons for the roughly thirty minute test cycle are emitted during the first two minutes of the test [2]. During this time the intake valve and port wall temperatures are low and it is thought that liquid fuel entering the combustion chamber results in the increased HC emissions. [2] [4].

Furthermore, a ULEV-certified engine emitted nearly two-thirds of the SULEV2 allowable hydrocarbons in the first five seconds of the same test cycle [5]. During this time the catalyst is below its activation temperature resulting in high tailpipe out emissions. Thus, when the intake valve and port walls are cold and the catalyst has not yet reached operating temperature, there is significant opportunity for reducing hydrocarbon emissions through the physical mixture preparation mechanisms.

1.3 Fuel economy benefits of load control via variable valve timing and lift

The possibility of near-term production engines including some form of variable valve control has allowed valve lift and timing to be additional variables in this study. The fuel economy impact of "throttle-less" load control via valve timing and lift is briefly reviewed below.

To first order, a fixed engine output will require a fixed mass of charge in the combustion chamber. The logic behind throttle-less load control is to close the intake valve such that the required mass of charge is trapped in the combustion chamber. Using the ideal gas law,

$$m_{trapped} = \frac{p_{intake} V_{IVC}}{R T_{intake}},$$

where $m_{trapped}$ is the trapped mass in the combustion chamber, p_{intake} is the intake absolute pressure, V_{IVC} is the volume of the combustion chamber at intake valve closing, R is the ideal gas constant for the air-fuel mixture, and T_{intake} is the intake temperature. It should be noted that a given value of V_{IVC} can be obtained by closing the intake valve during the intake stroke (early IVC) or during the compression stroke (late IVC). The denominator in equation 1.1 is essentially constant, so to obtain a given trapped mass one can raise the intake pressure and reduce the volume at IVC through valve timing. This reduces the pumping work in the engine cycle while at the same time reducing the effective compression ratio.

As mentioned above, the foremost benefit of load control via valve timing is the reduction of gas exchange pumping losses [6] [7]. Depending upon how variable valve timing and lift is implemented, there can also be reductions in engine friction and accessory work [8] [9]. However, there are other impacts on the engine cycle, in particular a degradation of combustion quality [7] [10] [11] [12].

The most significant source of combustion deterioration is lower charge temperatures at the time of ignition [7] [11] [13]. This reduction can be attributed to a lower effective compression ratio. For example, with an early IVC strategy, an expansion occurs before the compression stroke that lowers the charge temperature. Then, the polytropic rise during the compression stroke begins (and ends) at a lower temperature [9]. To some extent, the charge temperature at ignition can be positively influenced by valve timing through internal EGR via increased overlap, although the increased residual gas fraction may slow the combustion process and make it less stable.

At lower loads (and thus smaller required effective compression ratios and charge temperatures), several investigators have found it necessary to throttle the intake to obtain optimum fuel consumption [11] [13] [14]. In other words, eventually the benefits of reduced pumping work become overshadowed by the penalties of poor combustion quality.

A second source of combustion quality deterioration that has been identified for early IVC strategies is lower mean flow velocities and turbulence intensities in the combustion chamber at the time of ignition [7] [14]. The intake-generated flow has been measured to deteriorate before the end of compression. However, other investigators have observed improved combustion with early IVC strategies that they *deduce* is due to the persistence of intake generated flow *despite the effects of lower charge temperatures* [6] [11] [15]. These results may depend on other engine design variables such as the combustion chamber geometry.

A method of separating the effect different valve timings have on both the gas exchange process and the high pressure portion of the engine cycle is described in reference [16].

1.4 Previous work

Mixture preparation benefits of a variable valvetrain have been observed both indirectly and directly. Two manufacturers reported that significantly less enrichment – up to half the previous amount – was required for a cold start with their new variable valvetrains [6] [17].

In bench flow tests, significantly improved atomization has been observed with lower valve lifts. This effect is attributed to the increased velocity (and thus increased shear rates) through the valve gap [9]. For example, in going from 8 mm lift to 2 mm lift the average fuel droplet diameter was found to decrease from 157 μm to 9 μm [8]. At lower lifts the valve gap has been observed to act like an "atomizing sprayer" as any drops generated upstream burst in the gap due to aerodynamic forces [15].

Both direct visualization and quantitative measurements of liquid fuel droplets have been used to identify physical mixture preparation mechanisms. The mechanisms identified are (1) strip atomization, (2) spray contribution, (3) fuel film squeezing, and (4) deposition of liquid fuel films on the valve and head [18] [19]. Strip atomization is the process by which high velocity airflow past a liquid fuel film on the port wall or valve strips off droplets. The spray contribution is the liquid fuel droplets that were created by the fuel injector and remained suspended in the intake system. Fuel film squeezing occurs at intake valve closing and squeezes the fuel out of the valve seating surfaces, producing drops in the intake port and combustion chamber. Finally, liquid fuel films were observed to form on the valve and head, suspected to be due to the creation of recirculation regions around the valve.

1.5 Overview

This thesis focuses on identifying and understanding, on a fundamental level, the mixture preparation mechanisms for a port fuel injected engine. To that end, the logic used to design the experiments is presented in Chapter 2. The experimental apparatus and procedure are described in Chapter 3. Chapter 4 presents the results of the experiments in the form of the identified mixture preparation mechanisms. Chapter 5 summarizes these results and draws conclusions from them.

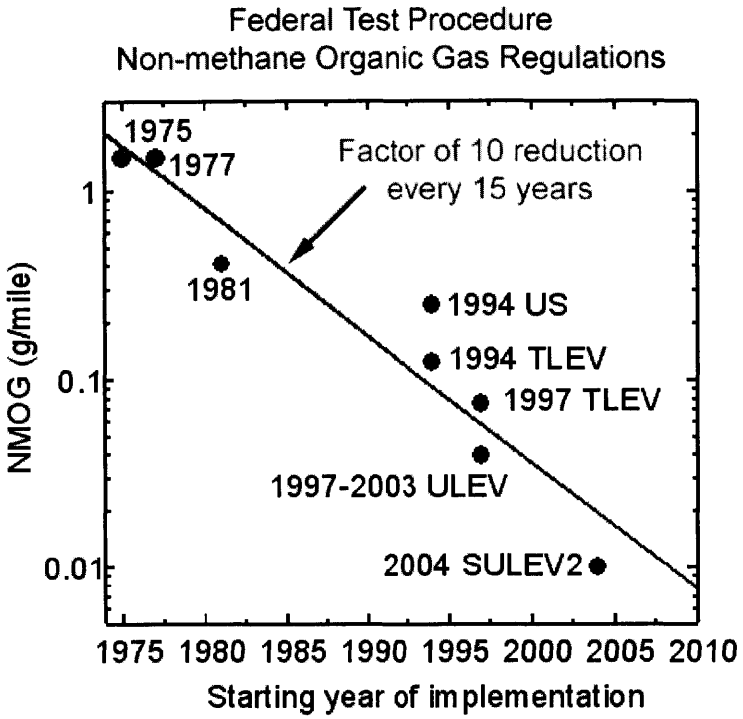

Figure 1.1: FTP non-methane organic gas regulations vs first year of implementation

2 Experimental Design

In designing the experiments, the goal was to produce a significant range of intake flow and fuel injection phenomena that would result in observable differences in the mixture preparation mechanisms. The decisions made during this process were driven by the desire for this study to be fundamental in nature.

2.1 Apparatus selection

A visualization engine was chosen for this study, as opposed to a bench flow rig, because many of the phenomena present in a firing engine, such as the backflow of hot residual gases into the intake port and correct component temperatures, can not easily be reproduced in a flow rig.

2.2 Valve timings

The definitions of valve opening and closing angles are complicated by the fact that the valve lift profiles begin and end with gradual ramps to reduce opening and closing impact forces. Typically, these are defined based upon a specified valve lift. Three common lifts that are used for this definition are zero (i.e. the true opening and closing angles), 0.006 inch, and 0.050 inch. The SAE standard is 0.006 inch and the preferred definition for performance manufacturers is 0.050 inch. It should be noted that all of the above lifts are lash-adjusted values and so are the actual lift at the valve and are not directly measured from the cam profile.

The exhaust valve timing and lift were fixed for these studies. The values used in the most recent studies using this engine were maintained [20]. The exhaust valve lift was 6.2 mm. The exhaust valve opening angle was 48° bBDC and the closing angle was 12° aTDC, both based on a zero lift definition. The exhaust valve open duration is 218° based on a 0.006 inch lift definition and 178° based on a 0.050 inch definition.

Figure 2.1 shows the normalized piston speed and the intake valve timings chosen for this study. The open duration was chosen to have the same period as the piston speed, disregarding the gradual opening and closing. This open duration is 220° at zero lift, 212° at 0.006 inch lift, and 168° at 0.050 inch lift[1].

The first valve timing chosen was an intake valve opening angle of 5° bTDC, based on a zero lift definition. Note that the valve lift profile is slightly out of phase with the piston speed. Normal intake valve opening angles are in the range of 10 to 25° bTDC and are chosen for fixed-cam engines as late as required to obtain acceptable idle quality [21]. Because previous studies

[1] To get a sense of how gradual the valve opening and closing is, without the specified 0.1 mm lash the open duration at zero lift becomes 265°.

using this engine used an intake valve opening angle of 5° bTDC this value was maintained as a baseline. This opening angle provides a moderate amount of valve overlap. The overlap factor for this timing is 0.77 °/mm^2.

The second valve timing was chosen to be almost exactly in phase with the piston speed. This resulted in an intake valve opening angle of 25° bTDC based on a zero lift definition. There is significantly more overlap with this valve timing. The overlap factor is 6.61 °/mm, nearly an order of magnitude larger than the first valve timing.

The final valve timing was chosen to be significantly out of phase with the piston speed. By the time the piston has reached roughly half of its maximum velocity, the valve is just beginning to open. The intake valve opening angle for this timing was 25° aTDC. No valve overlap is present with this timing.

In subsequent sections of this thesis, the 25° bTDC, 5° bTDC, and 25° aTDC intake valve timing will be respectively referred to as "early," "intermediate," and "late."

To verify that these valve timings would produce a suitable range of flow characteristics, as well as to determine the intake valve lifts to be used in the study, an engine cycle simulation study was carried out.

2.3 Intake valve lifts

It was expected that the most significant physical factor affecting mixture preparation would be the valve gap velocity. Thus, an engine cycle simulation was used to predict the valve gap velocity histories for several lifts at each of the valve timings above.

The engine simulation package WAVE by Ricardo Software was used to perform this analysis. Figure 2.2 shows the graphical representation of the WAVE model. In order to study the engine cycle itself in the absence of any tuning effects, the intake and exhaust conditions were specified as fixed boundary conditions. Because the primary interest was in cold engine conditions, all component temperatures were specified as ambient. All other inputs to the model were matched to the square piston engine geometry.

It should be noted that although an injector is present schematically in the model, the injector behavior itself is not modeled. For the purposes of this analysis, it was assumed that a

[2] A common means of quantifying the amount of valve overlap is the overlap factor, which is defined in detail in the appendix of reference [22]. For equal intake and exhaust valve diameters, it is simply a scaling of the area under the exhaust and intake lift profiles during valve overlap. This definition is thought to be more meaningful than simply specifying the overlap duration in crank angles.

uniform stoichiometric mixture entered the combustion chamber, and the injector was specified accordingly.

The valve gap velocity is not an available output from WAVE. It was computed from the mass flow rate into the combustion chamber $\dot{m}$, the in-cylinder and intake densities ρ, and the effective valve open area A_{eff} as:

$$v = \frac{\dot{m}}{\rho A_{eff}}.$$

Depending upon the direction of $\dot{m}$, the intake or in-cylinder density was used. This method of determining the valve gap velocity was chosen (as opposed to determining the Mach number of the flow from the pressure ratio or assuming incompressible flow) because WAVE includes proprietary corrections for unsteady compressible flow.

Figure 2.3 and Figure 2.4 show the results of these simulations at 1000 RPM for intake pressures of 0.5 bar and 1.0 bar respectively. Note that due to much higher backflow velocities with lower intake pressures, the scales of the two plots are not the same.

Particularly when there is backflow, the initial flow history is relatively insensitive to the valve lift because the flow is sonic. Once the combustion chamber and intake pressures equilibrate, the flow history is insensitive to intake pressure as the mass exchange process becomes driven by piston displacement.

Each of the valve timings chosen produce very different flow characteristics. Roughly speaking, the shapes of the velocity histories at each valve timing are similar. The early timing has a significant initial backflow duration with a relatively constant forward flow history. The late timing has little or no initial backflow and continually decelerates from a near sonic peak forward flow. The intermediate timing is in between these two: a moderate duration initial backflow and a more gradual deceleration from a peak forward flow velocity.

The valve lifts used in this study were chosen based on these simulation results. The existing intake valve lift on the engine was 6.2 mm. Because they increase valvetrain stresses, for mechanical reasons larger lifts were not considered. A 1 mm valve lift produces flow velocities very similar to a 2 mm lift, as both are nearly sonic throughout the entire open duration. Because a lift of 1 mm would require a rocker ratio twice as large (which is challenging to implement) and would not produce any significantly different flow characteristics, a 2 mm lift was chosen along with 6.2 mm lift to be the primary lifts used in this study.

2.4 Injection timing

Both closed- and open-valve injection timings were used in this study. Based on early visualization in the intake port, a closed-valve start of injection of 65° after intake valve closing was chosen. This timing was as early as possible while allowing sufficient time for intake valve closing phenomena to be observed in the intake port before the port became obscured by the

injected spray. An open-valve start of injection of 40° aTDC-intake was chosen for all valve timings because at this point all of the flow velocities are forward and sufficiently large. (See Figure 2.3 and Figure 2.4; 40° aTDC-intake is 400° on the plots)

2.5 Fuel injectors

Two fuel injectors provided by Delphi Corporation were used for this study. The first injector is typical of current production injectors. It is four-hole injector with a 20° cone angle and a Sauter Mean Diameter (SMD) of 63 μm and a D_{V90} of 171 μm, measured at 330 kPa fuel system pressure [3]. This injector provides relatively good atomization and deposits fuel on the intake valve as well as the intake port walls. The second injector provided very poor atomization and deposited nearly all of the fuel as a liquid at the valve. It has a 4° cone angle and a Sauter Mean Diameter of 184 μm and a D_{V90} of 500 μm, measured at 300 kPa fuel system pressure. Both injectors had similar flow characteristics and thus similar injection durations: the one hole injector had a static flow of 2.37 g/s at 300 kPa fuel system pressure, while the four-hole injector had a static flow of 2.2 g/s at 330 kPa fuel system pressure.

Assuming a Rosin-Rammler distribution [23], the droplet distribution for the two injectors is shown in Figure 2.5. Injectors that produced droplet distributions slightly better than the four-hole injector (e.g. a six- or eight-hole injector) were not used in this study because it was difficult to visually discern any differences in the injected sprays.

2.6 Diagnostic method

In order to study the mixture preparation process on a fundamental level, a diagnostic method was desired that was capable of showing within a single engine cycle the development of phenomena in a large field-of-view. The natural choice was high-speed videos. Unfortunately, it is difficult to be quantitative with the videos. However, many quantitative techniques tend to be local point-based measurements, such as phase Doppler particle anemometry (PDPA). Furthermore, other techniques can only observe a single plane of view, such as planar laser-induced florescence (PLIF). With both of these techniques, it is difficult to observe the interactions that occur during the mixture preparation process, which was primary goal of this study. Thus, high speed videos were determined to be the most suitable diagnostic method.

[3] The Sauter Mean Diameter is useful for characterizing the average evaporation of a spray. It is the diameter of a droplet whose volume to surface area ratio is equal to the total volume of the spray divided by the total surface area of the spray. The D_{V90} is useful for characterizing complete evaporation of a spray. 90% of the volume of the spray is contained in droplets smaller than the D_{V90}.

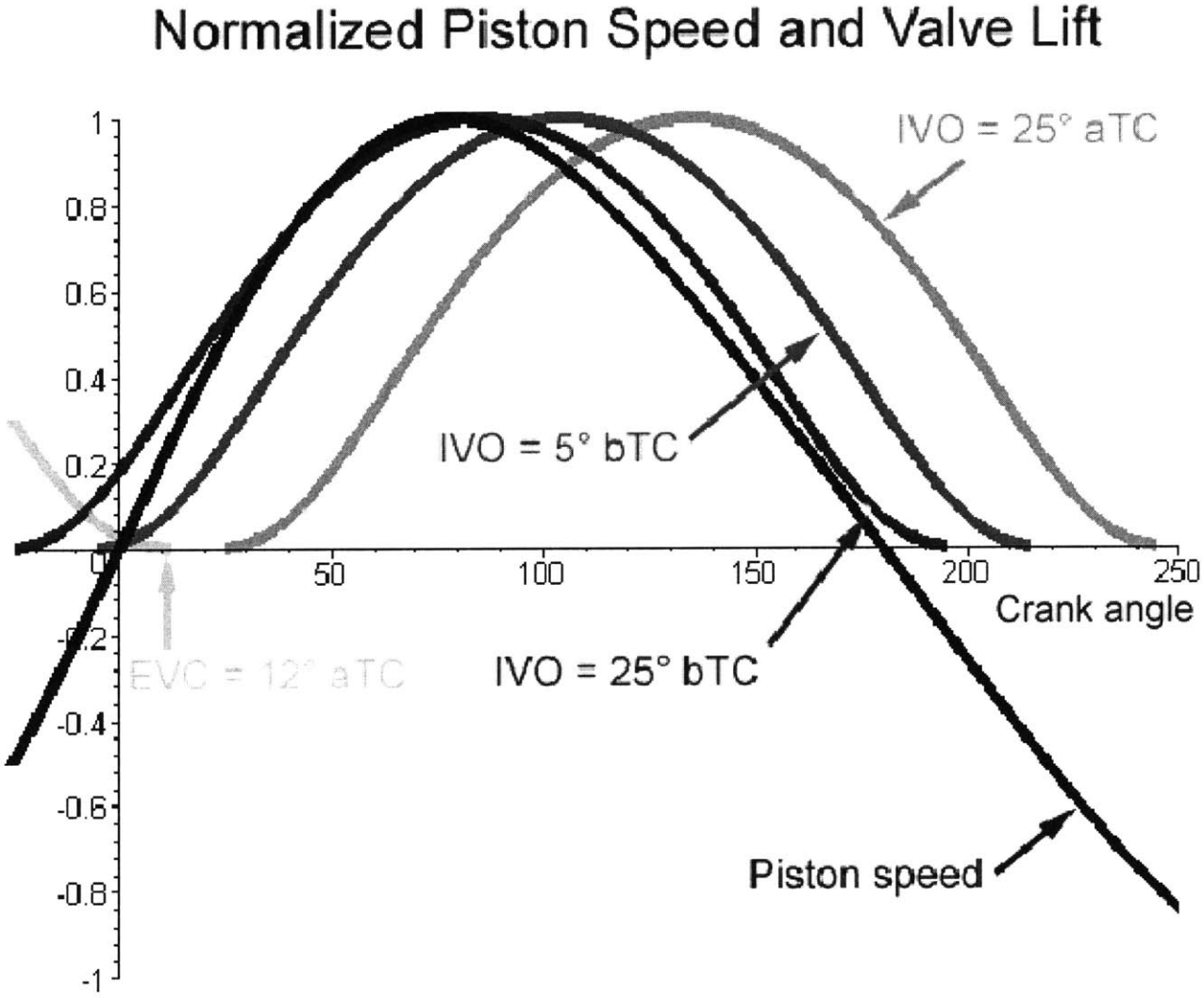

Figure 2.1: Normalized piston speed and valve lift for the three valve timings

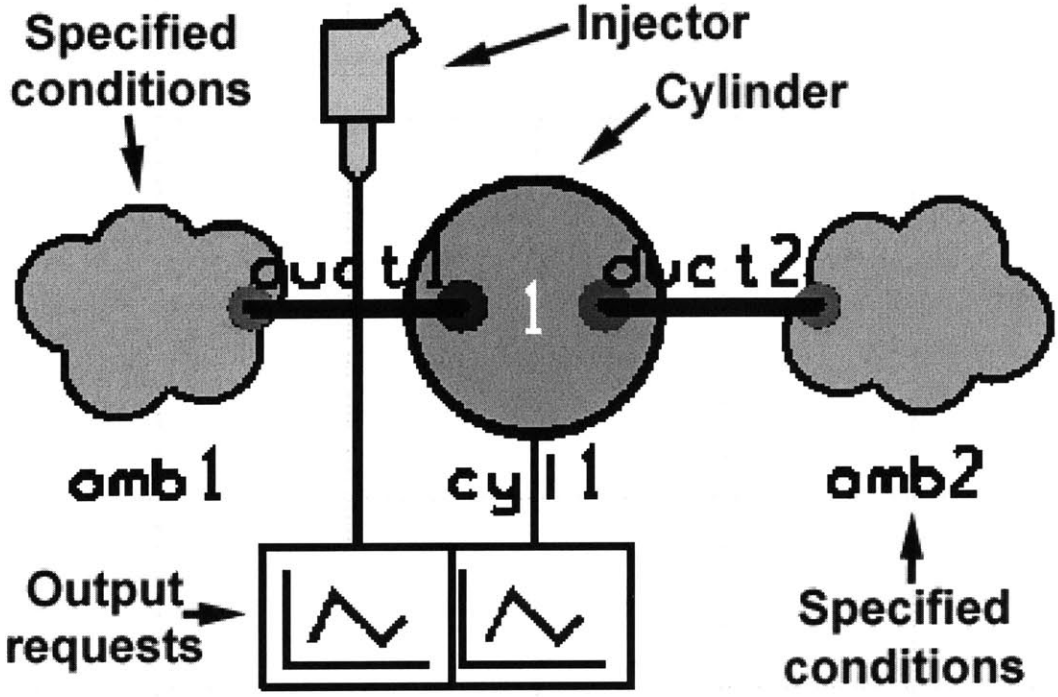

Figure 2.2: Wave model used for engine cycle simulations

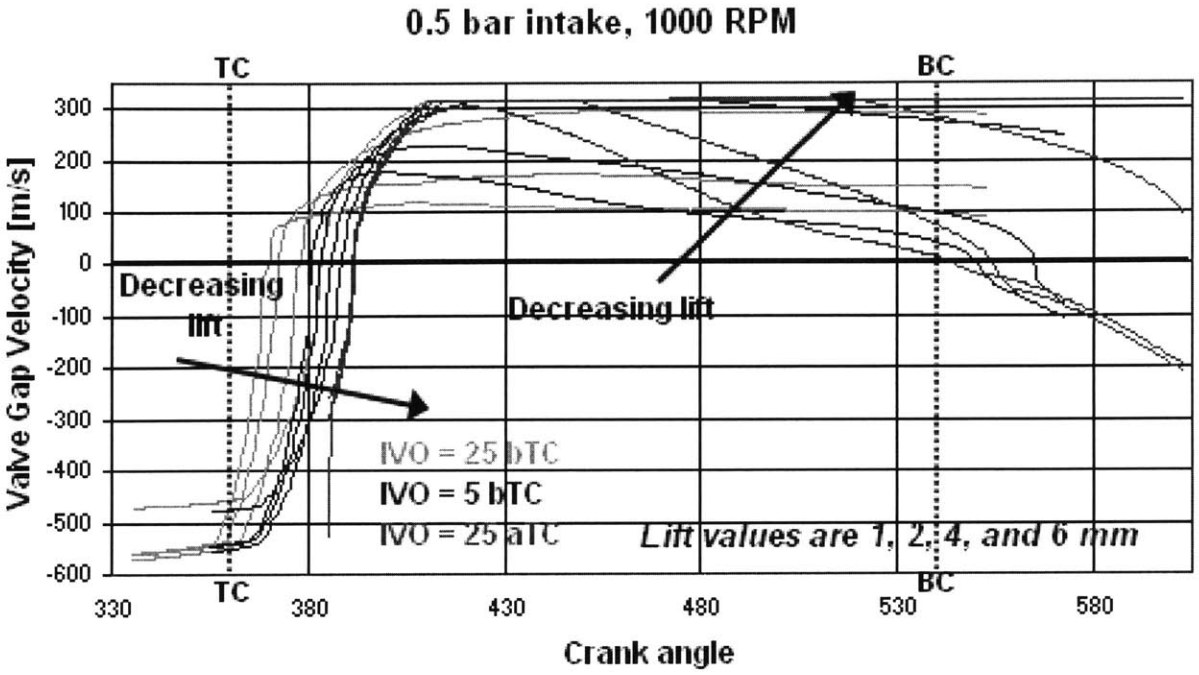

Figure 2.3: Simulated valve gap velocities for the square piston engine at 1000 RPM and 0.5 bar intake pressure

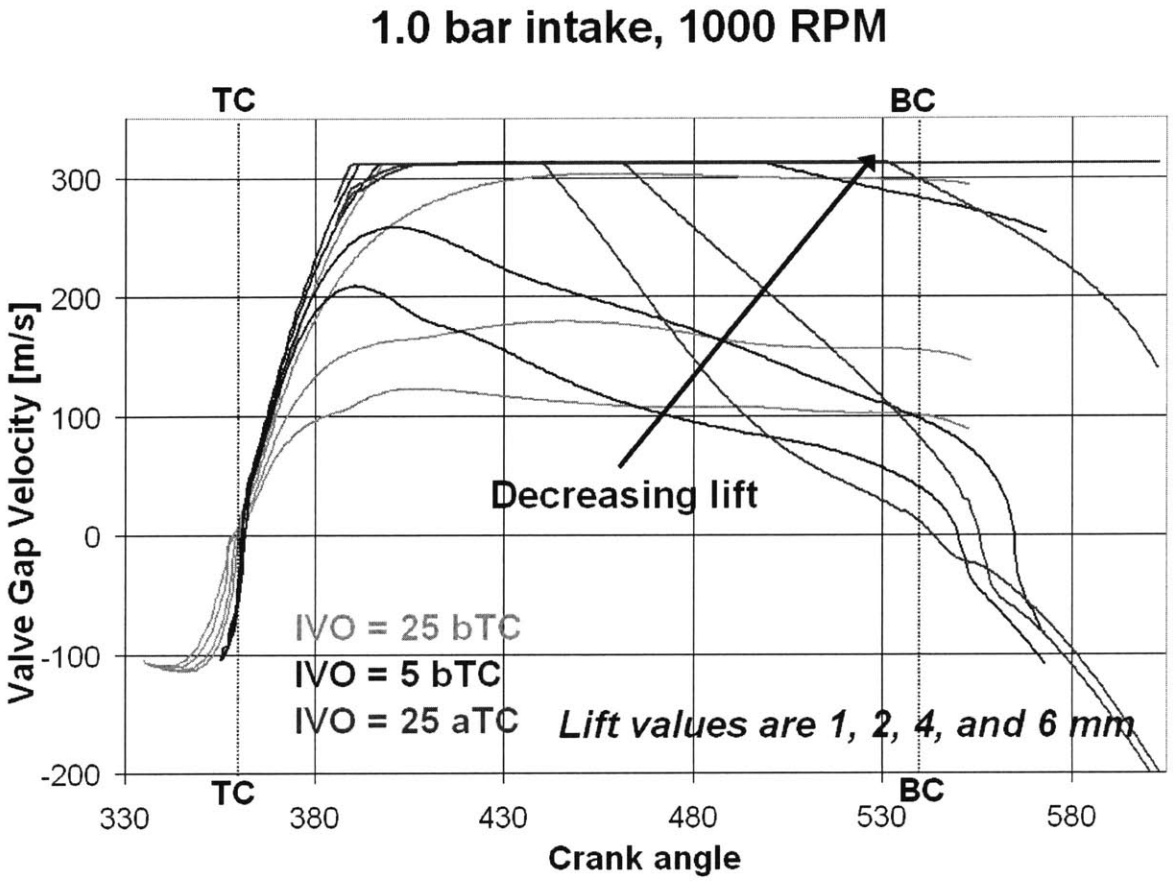

Figure 2.4: Simulated valve gap velocities for the square piston engine at 1000 RPM and 1.0 bar intake pressure

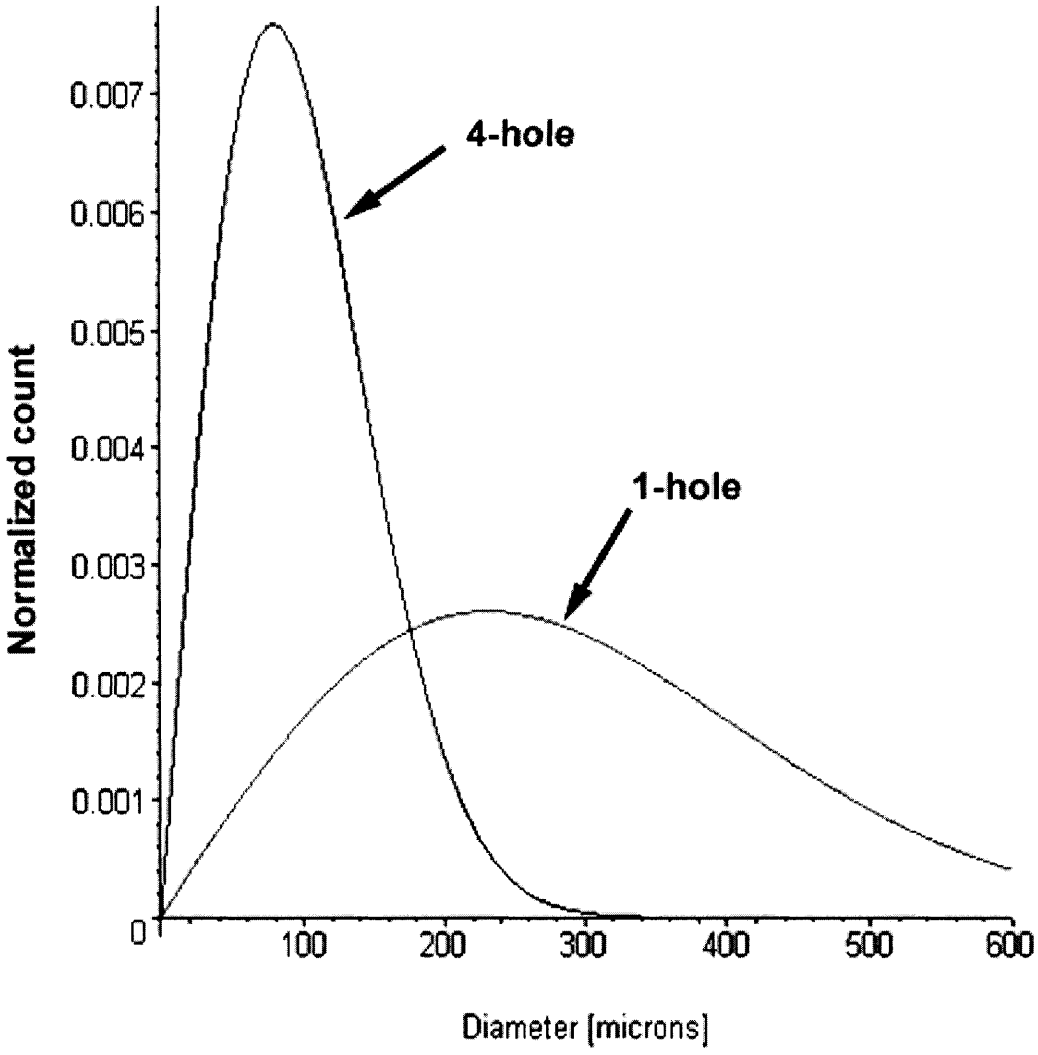

Figure 2.5: Rosin-Rammler droplet distributions for the two injectors.

3 Experimental Setup

3.1 Visualization engine

Figure 3.1 shows a schematic of the visualization engine used in this study. This engine is special in that the bore is square and two of the combustion chamber walls are made of quartz. The square combustion chamber allows for undistorted optical access. The quartz walls can be removed and cleaned between experiments.

Good optical access does come at the cost of more challenging engine sealing. The rubber gaskets used to seal the windows must be replaced every few experiments. Graphite bars are used to provide a dry means of sealing the combustion chamber so that the windows are not fouled by lubrication oil. These bars overlap at the corners and are pressed against the combustion chamber walls by small springs.

Figure 3.2 shows a schematic of the intake port of this engine. It should be noted that this engine was previously converted from carburetion to port fuel injection, thus the nonstandard intake port geometry. The inner radius of the port was removed to allow for better targeting of the injected spray on the back of the intake valve. This modification is not expected to significantly alter any of the mixture preparation mechanisms as the primary mechanisms are thought to occur around the intake valve gap where the flow velocities are highest.

Details of the engine configuration are given in Table 3-1.

3.2 Rocker arms

In order to vary the intake valve lift, rocker arms of varying rocker ratios were created rather than changing camshafts. This was primarily for practical reasons. The rocker arms were external and could be changed in roughly ten minutes, while changing the camshafts required complete engine disassembly and took roughly six hours.

It should be noted that initially it was thought that varying the valve lift via the rocker ratio would not produce valve events consistent with production variable valve control mechanisms. Ideally, one would like the mechanism to simultaneously reduce lift and open duration. However, based on competitive analyses, several production variable valve timing and lift systems do indeed maintain longer open durations at reduced lift [24].

The existing rocker arms produced an intake valve lift of 6.2 mm. New rocker arms were designed that provided 2, 3, 4, and 5 mm of lift. Figure 3.3 and Figure 3.4 are photographs of these rocker arms. For details of the rocker arm design process and other valvetrain modifications refer to Appendix 1.

3.3 High-speed camera

The high-speed CMOS camera used in this study was the monochrome version of the Phantom v4.2 made by Vision Research. The monochrome version was chosen due to its increased light sensitivity.

At full resolution of 512x512 pixels, the camera is capable of up to 2100 frames per second. As resolution is decreased, the maximum frame rate increases. For example, at 32x32 resolution the maximum frame rate is 90000 fps; at 256x128 resolution the maximum frame rate is 7100 fps. For reference, 7100 fps corresponds to roughly 1.2 frames per crank angle at 1000 RPM.

The camera is controlled via a personal computer running the manufacturer's camera control software. The desired portions of the videos are transferred from the camera to the computer and stored digitally on the computer's hard drive. Communication between the camera and the computer occurs through an Ethernet cable.

3.4 External lighting

Two Lowel Tota-Lights with 650 watt tungsten halogen bulbs were used to illuminate the combustion chamber for the in-cylinder videos. These lights were chosen because they provide a relatively broad throw of light to uniformly illuminate the combustion chamber. A particular advantage of the halogen bulbs is that the light they provide is incoherent – has no preferred direction, amplitude, or phase – and thus will scatter more uniformly [25]. This is important in order to more clearly observe the light reflected and refracted by the fuel droplets in the combustion chamber.

Figure 3.5 shows the halogen lights and high-speed camera setup for in-cylinder videos. The halogen lights are aligned perpendicular to the windows while the camera is offset at an angle to avoid any light from either of the lamps reflecting directly into the camera. In this way, the light reflected and refracted by the fuel droplets is not "overpowered" by the light coming directly from the lamps.

Figure 3.6 shows the actual field of view for the in-cylinder videos. In the photograph, the intake valve is located in front of the exhaust valve, which is only partially viewable. Some liquid fuel accumulation is evident as darker regions on the intake valve and head. Also visible are the spark plug and in-cylinder pressure transducer.

3.5 Borescope

An Olympus Series 5 rigid borescope, model number R080-024-090-50, was used to capture videos in the intake port. The high-speed camera was connected to the borescope using a special adapter, Olympus part number AK2-10C. Illumination through the borescope was provided with a liquid light guide cable and a Xenon high-intensity light source, Olympus model ILX-6300.

Figure 3.7 shows the borescope and high-speed camera setup for intake port videos. As is shown schematically in Figure 3.8, the borescope body runs the length of the intake manifold and ends near the valve guide in the intake port. The borescope was positioned to one side in the intake manifold (approximately 9 o'clock if one is looking down the intake manifold toward the port) to avoid interfering with injected fuel spray. A small area of the valve guide was machined out to ensure repeatable positioning of the borescope, as well as to provide a slightly better view of the intake valve. The location at which the borescope entered the intake manifold was sealed with nylon Swagelok fittings to protect the borescope body while still providing adequate sealing.

The borescope is aimed at the intake valve and port wall on the injector side of the port. Figure 3.9 shows the actual view through the borescope. Also visisble is a fast-response thermocouple used to measure the intake valve temperature.

3.6 Engine control

A previously developed LabView-based engine control system was used to operate the engine[4]. LabView is a data acquisition and signal control software package made by National Instruments. This engine control system consists of a personal computer running LabView with a National Instruments PC-TIO-10 timing board.

The engine controller receives as inputs a crank angle signal and a once-per-cycle bottom dead center signal. It outputs control signals for the fuel injector and ignition coil. The ignition timing, injection timing, and injection duration are set in software by the user.

Due to hardware limitations, the ignition timing, injection timing, and injection duration can not be modified on a cycle-to-cycle basis. In order to get the engine firing relatively quickly, a fuel enrichment module was added separately from the engine controller. This circuitry enriches the very first fuel injection event by a user-set amount. For all of the experiments conducted, this amount was set to roughly eight times the stoichiometric amount.

[4] For more information, refer to Mike Shelby's SM thesis (May 1997). Minor modifications were made by Brad VanDerWege and are documented in his PhD thesis (May 1999).

3.7 Data acquisition

National Instruments data acquisition hardware and software were used to record various engine operating variables. The data acquisition system consisted of a personal computer running LabView with a PCI-6024E multifunction data acquisition card. This card can read up to 200,000 samples per second. It is limited, however, to eight differential channels of input. To overcome this limitation, an SCXI-1000 multiplexing chassis was also used.

The SCXI chassis houses up to four signal conditioning modules and multiplexes all of their channels into one channel on the data acquisition card. Three modules were used: a thirty-two channel analog input module (SCXI-1100) attached to a terminal block (BNC-2095), an eight-channel thermocouple input module (SCXI-1112), and a feedthrough panel (SCXI-1180) attached to a terminal block (SCXI-1302) for accessing the digital I/O lines on the data acquisition card. The thermocouple module includes a built-in 2 Hz filter for eliminating noise from thermocouple measurements. Due to hardware limitations, the analog inputs could not be filtered.

The data acquisition card can not simultaneously acquire data at multiple speeds. Thus, all of the data acquired in these experiments was taken once per crank angle. Some of the data was post-processed to obtain a cycle-average value.

3.8 Instrumentation

A Meriam Instruments laminar flow element (model 50MW20-1 1/2) was used along with an Omega low differential pressure transducer (model PX2300-1DI) to measure airflow through the engine. The output of this pressure transducer was not logged using the data acquisition system. The output of all other instruments described below was logged.

A Honeywell absolute pressure transducer (model SA015PA1C1D) was used to measure the intake manifold absolute pressure. This transducer has a 0.5 ms response time (five time constants are roughly 15 crank angles at 1000 RPM). This response is sufficient to obtain an average manifold pressure around bottom dead center of the compression stroke in order to reference the cylinder pressure measurement.

A water-cooled Kistler pressure transducer (model 7061) was used to measure the in-cylinder pressure. A Kistler model 5004 charge amplifier was used to convert the output of the pressure transducer into a voltage that could be logged by the data acquisition system.

A Horiba MEXA-110λ universal exhaust gas oxygen (UEGO) sensor was used to measure the air-fuel ratio. These sensors have typical maximum response times on the order of 100-150 ms. This corresponds to roughly one cycle at 1000 RPM.

Omega fast-response thermocouples (type CO-1) were installed on the intake valve. These thermocouples have a response time of 20 ms (five time constants are roughly 600 crank

angles at 1000 RPM). Thus, cycle-to-cycle valve temperatures can be determined. Two thermocouples were installed on the valve, one "shadowed" from the injector by the valve stem and one diametrically opposite it.

3.9 Experimental procedure

In all experiments, the engine began at ambient conditions. In order simulate a warmup (but not starting) process, the engine was motored to the desired speed. Once the airflow through the engine stabilized, fuel injection was initiated immediately. The camera was then triggered during the desired phase of engine operation.

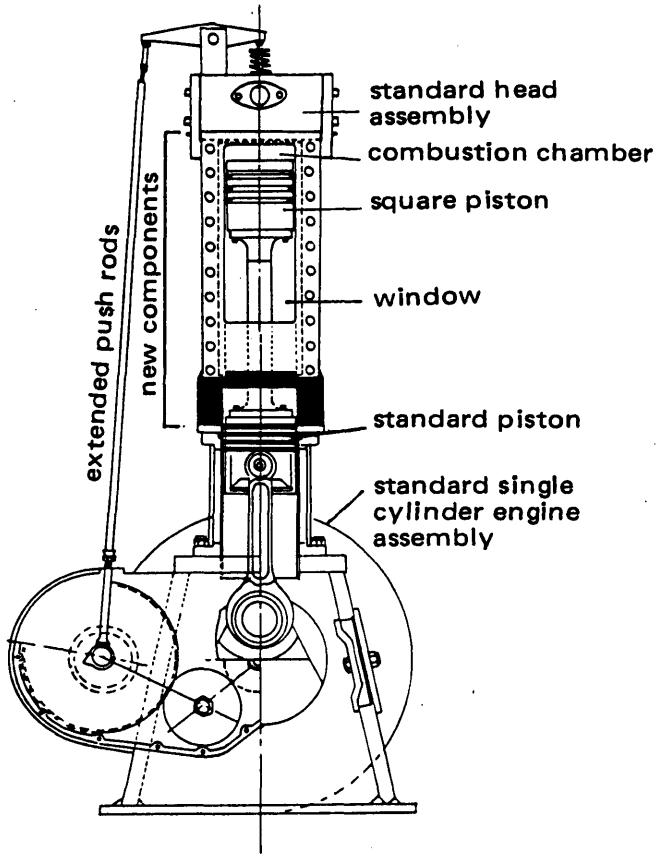

Figure 3.1: Schematic of the square piston visualization engine

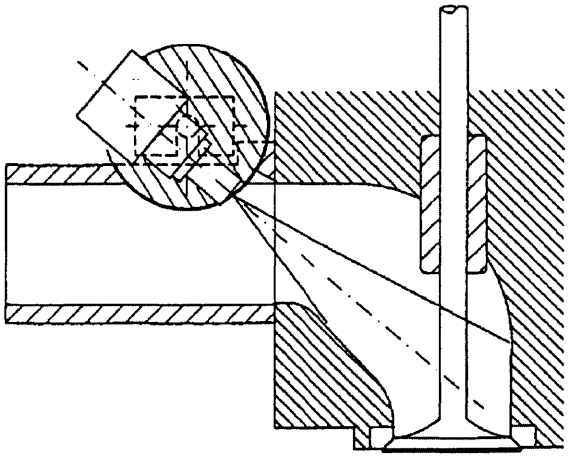

Figure 3.2: Square piston engine intake port schematic

Displaced volume	**785 cm^3**
Effective bore*	**93.5 mm**
Stroke	**114.3 mm**
Connecting rod length	**254.0 mm**
Compression ratio	**8.0**
Number of intake valves	**1**
Intake valve diameter	**32.0 mm**

Table 3-1: Configuration details of the square piston engine
**** Effective bore is defined as the bore of a circular cross-section piston with an equal area as the square piston***

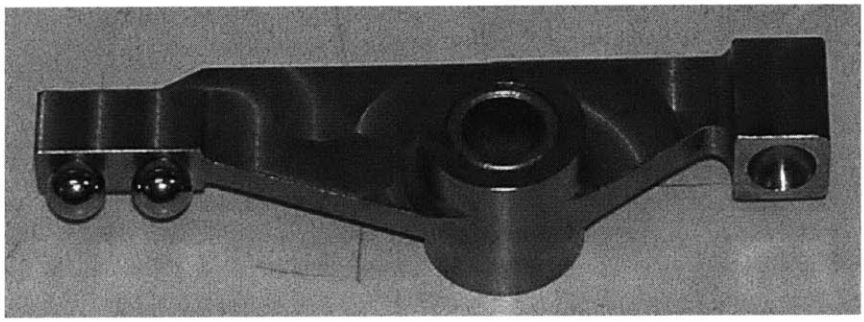

Figure 3.3: Photograph of the 5 and 4 mm lift rocker arm

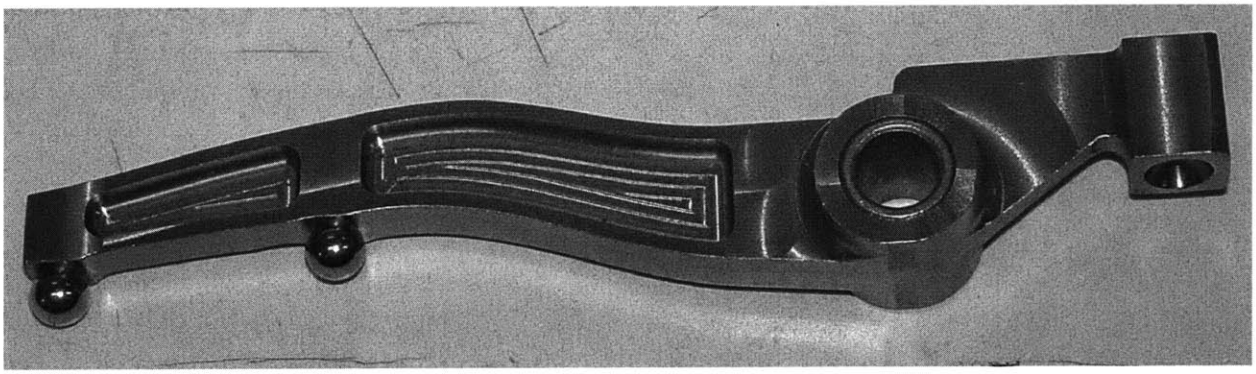

Figure 3.4: Photograph of the 3 and 2 mm lift rocker arm

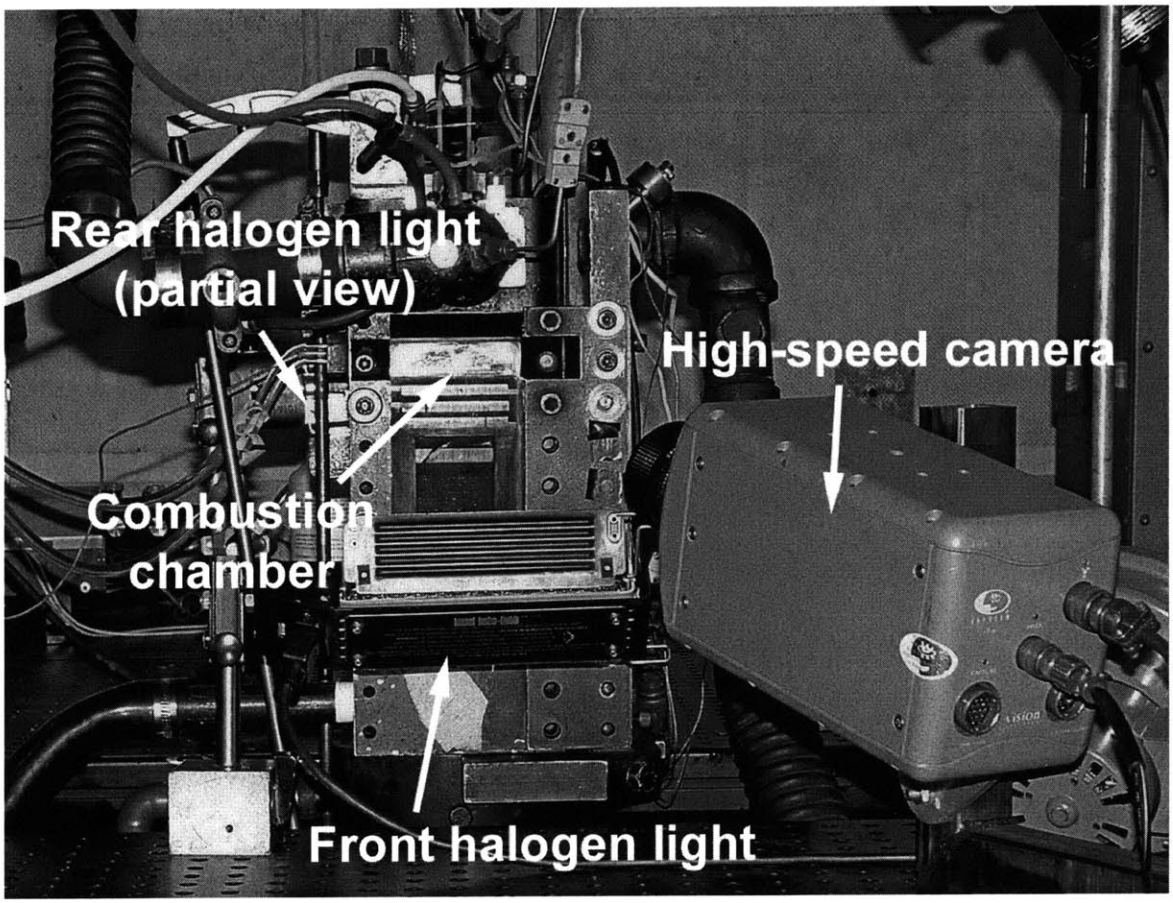

Figure 3.5: Photograph of in-cylinder video setup

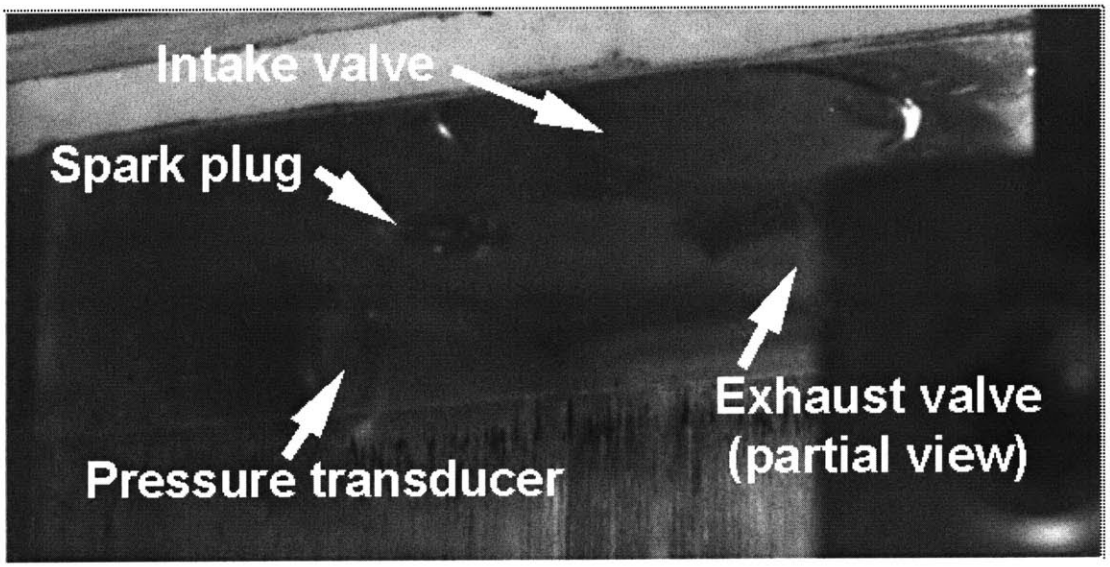

Figure 3.6: Actual field of view for in-cylinder videos

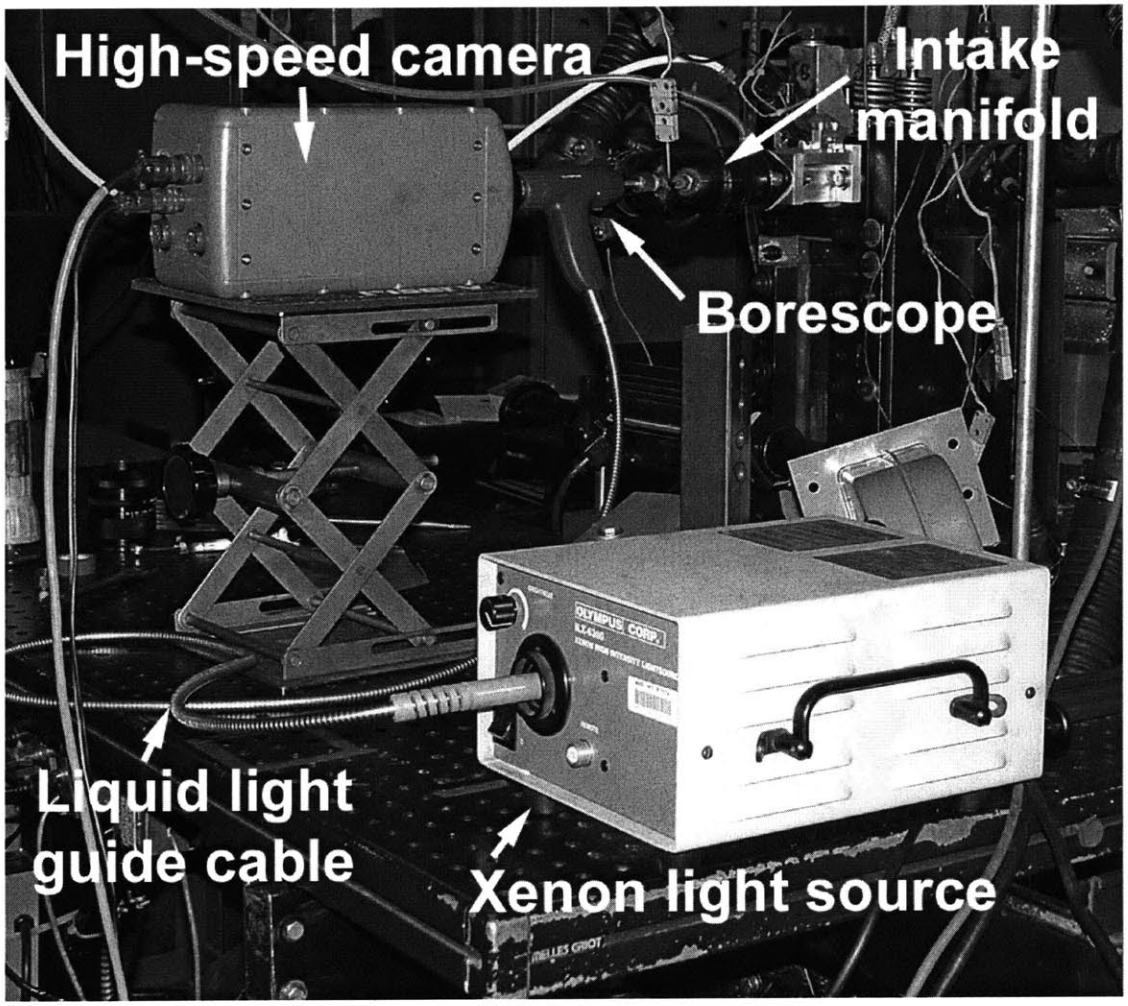

Figure 3.7: Photograph of the intake port video setup

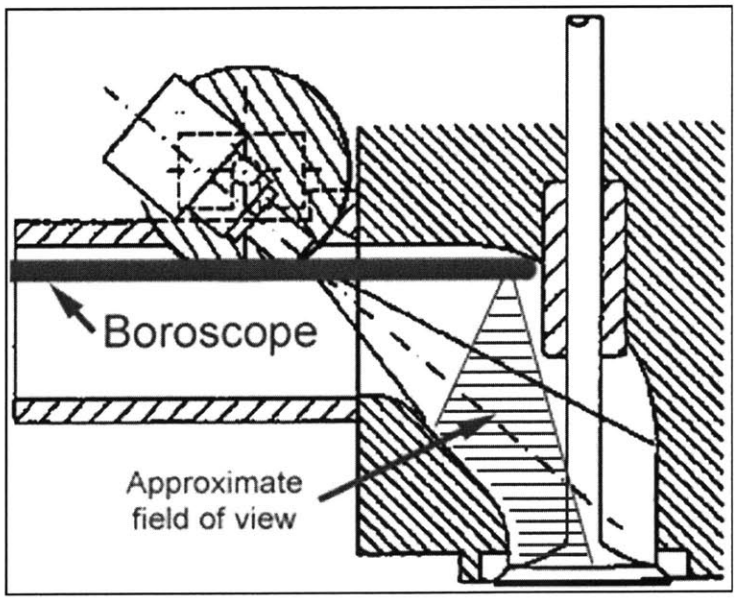

Figure 3.8: Schematic of borescope location in the intake port and manifold

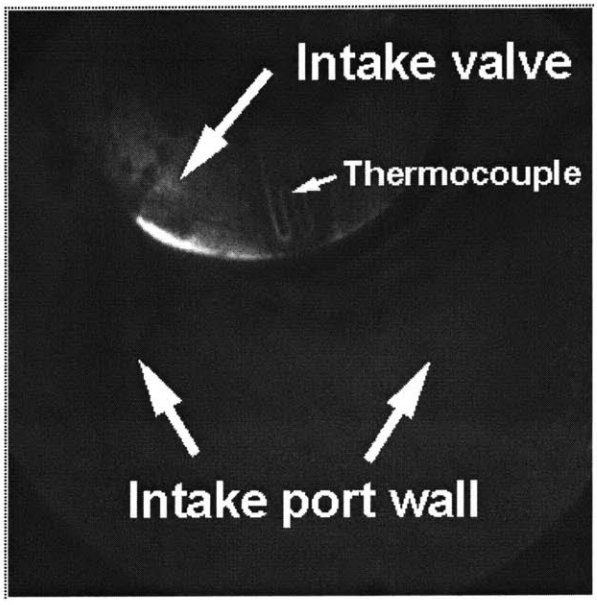

Figure 3.9: Actual field of view of the borescope

4 Results and Discussion

High-speed videos were used to study the mixture preparation mechanisms. Every attempt has been made to clearly depict these mechanisms by showing representative frames from the videos. The ability to observe these mechanisms progress in time is lost, however, when only showing individual frames. Furthermore, some mechanisms are very difficult to depict in still frames. For this reason, a CD containing selected videos from this study has been submitted with this thesis and will be referred to below.[5]

The videos are in the Microsoft Windows uncompressed AVI format and should be viewable using standard video software (such as Windows Media Player) on any personal computer. A Windows XP freeware utility to adjust the frame rate (for faster or slower playback) is also included on the CD. Depending upon the ambient lighting, it may be helpful to adjust the contrast and brightness of the screen while watching the videos.

The mechanisms that were identified can be classified as either transport mechanisms or conversion mechanisms. The transport mechanisms are the means by which liquid fuel enters the combustion chamber, either as droplets or films. The conversion mechanisms are the means by which droplets are converted to films (or vice versa) within the combustion chamber.

4.1 Operating conditions

For all of the experiments mentioned below, the operating conditions shown in Table 4-1 were used. In particular, note that all experiments were conducted at roughly constant load since the airflow and equivalence ratio are held constant.

Table 4-2 shows the operating conditions that were varied in the experiments. Note that since the intake pressure was reduced, it was not necessary to conduct experiments with the early valve timing since similar flow phenomena are obtained with the intermediate timing (see Figure 2.3).

4.2 Event diagrams

For each experiment, an event diagram was constructed that depicts, on a crank angle basis, the phenomena that occur in the intake port and combustion chamber. In order to aid in

[5] In some of the videos, a "bubbling" is visible in the intake port. In an earlier study, the intake port was modified to permit targeting of the injected spray on the back of the intake valve. The port was filled in with epoxy and there is a small crack in the epoxy near the valve. Because the intake manifold is below atmospheric pressure, a small amount of air leaks into the port and creates bubbles if a fuel film is across the crack.

interpretation, the simulated valve gap velocities are also included on the event diagrams. The event diagrams are shown in Figures 4.1 through 4.8.

It should be noted that there is a significant amount of blowby in this engine which is not included in the simulation model. This will have a considerable impact on the high pressure portion of the engine cycle, but only a minor impact on the intake process due to slightly lower burned gas temperatures resulting from lower combustion pressures, and thus lower-than-predicted backflow velocities at intake valve opening. The effect of the incomplete sealing is negligible during the intake stroke because the intake valve open area is significantly larger than the area through which the blowby occurs. Thus, although the blowby in this engine is not modeled, these simulations are still applicable.

4.3 Transport mechanisms

4.3.1 Strip atomization

Perhaps the most recognized mixture preparation mechanism, strip atomization is the process by which droplets are stripped from fuel films on the port wall or valve surface by high velocity flow. It is shown schematically in Figure 4.9. The actual droplet formation is difficult to observe, but the evidence of it is clear. Figure 4.10 (taken from the experiment 1 videos at roughly 100° aTDC intake) shows droplets entering the combustion chamber (small white spots in the valve gap) while also indicating the rippling of the fuel films on the valve and intake port wall in an otherwise clear port. The rippling of the fuel films in the intake port is especially clear in experiments 4, 5, 7, and 8.

Strip atomization also occurs during the high velocity backflow at intake valve opening. Figure 4.11 shows the conditions in the intake port during intake valve opening backflow, during forward flow, and just after the end of injection. The fact that the cloudiness in the port increases during backflow can be used to deduce that strip atomization has occurred, producing more droplets and making the port more "cloudy."

It should be noted that, in experiment 1, droplets are not observed to enter the combustion chamber during the end of the forward flow period. Likewise, strip atomization is not observed during intake valve closing backflow, although liquid fuel is present that participates in IVC film squeezing. Both of these facts can be attributed to the lower flow velocities present being insufficient to result in strip atomization.

Finally, strip atomization has also been used in previous literature [18] to describe the process by which a liquid fuel film is displaced along the valve or port walls and immediately breaks up into drops in the valve gap. The term "strip atomization" is also used here to describe this phenomenon.

4.3.2 Film displacement head wetting

In addition to resulting in strip atomization, the forward flow into the combustion chambers also displaces the films on the intake port walls, as is very clear in experiments 4, 5, 7, and 8. If the flow velocity is not sufficiently high, these films can simply flow onto the head as films, held together by surface tension. This phenomenon is shown in Figure 4.12. It is especially evident in experiments 1 and 2 around 120° after TDC-intake as shown in Figure 4.13. Note that no flow onto the head is observed for lower flow velocities.

4.3.3 IVC seat film squeezing

When the intake valve closes, any liquid fuel that is present around the valve seat will be squeezed out, either into the port or into the combustion chamber as droplets or as a film. In experiment 1, drops are squeezed both into the combustion chamber and into the intake port (Figure 4.14 and Figure 4.15). Note that the drops in the combustion chamber produced by the film squeezing remain suspended and completely evaporate during the compression stroke.

This film squeezing process does appear to be affected to some extent by the intake flow (see Figure 4.16), as evidenced by the fact that in experiments 4 and 7 there is a high velocity inflow at intake valve closing and both a film and droplets are squeezed into the cylinder, with the drops being projected at a lower angle than in experiment 1, which had a relatively low velocity backflow at intake valve closing. Furthermore, no film squeezing into the intake port is observed in these two experiments. This is not simply due to the more gradual closing with lower lifts because the squeezing phenomena in experiment 8 (also 2 mm lift) is similar to that of experiment 1 – note however that both have relatively low velocity flows at intake valve closing.

It should be noted that the nature of the IVC squeezing will likely be affected by the valve seating geometry. In this engine, the seating surfaces are a rather large band near the bottom of the valve. This is shown in Figure 4.17, which is a photograph of the valve after being lapped. The lighter region is the seating surface.

4.3.4 Valve head wetting

Whenever the intake flow velocity is low or reverses, there is the possibility for any liquid fuel present on the valve to be drawn by gravity around the seating surfaces and onto the valve head, where it remains as a film due to surface tension. This phenomenon was observed in all experiments in which there was a flow reversal from forward flow to backflow. It is shown schematically in Figure 4.18 and in Figure 4.19 for experiments 1, 2, 3, and 5.

4.3.5 Injection contribution

Even with closed-valve injection, some of the droplets created by the fuel injector remain suspended in the intake port until they enter the combustion chamber, as evidenced by the persistence of an overall cloudiness in the port after the fuel injection. This is shown schematically in Figure 4.20 and in Figure 4.21 for experiment 1.

With open-valve injection a much larger fraction of the liquid fuel that enters the combustion chamber is directly from the injector, as evidenced by the much finer mist entering the combustion chamber. Very little of this fuel settles on the port walls and valve, resulting in minimal valve and head wetting. See Figure 4.22.

With open valve injection the fuel spray is clearly influenced by the intake flow, despite the "large" size of droplets produced by the injector. This is most clearly seen in experiment 3, in which the injector-side port wall is not wetted while there is evidence of significant wetting of the opposite wall in the form of IVC film squeezing droplets. When the injector is fired upon a closed valve, as in experiment 1, the injector-side port wall is completely wetted.

4.3.6 Valve slide off

When there is a high velocity inflow through a sufficiently open intake valve, there is the possibility of flow separation occurring. If this happens, any fuel that was on the valve below the separated flow is free to slide or fall off the valve due to gravity. This phenomenon is shown in Figure 4.23. It is most clearly seen in experiment 5 around 60° after TDC-intake (where the valve gap flow velocity is maximum), as shown in Figure 4.24.

4.4 In-cylinder conversion mechanisms

4.4.1 Coalescence of drops on combustion chamber walls

Regardless of how they were created, any droplets that enter the combustion chamber can coalesce on the walls to form films. Experimentally it was extremely difficult to observe this process. For some of the experiments, photographs of the impingement patterns left on the quartz windows were taken. They are shown in Figure 4.25.

Clearly in experiments 1, 4, 5, and 7 a fuel film does end up on the combustion chamber wall. With experiment 3, it is unclear whether so little fuel impinges upon the window that it leaves no pattern or whether so much fuel impinges on the window that it washes away any

impingement pattern. From carefully observing the spray hitting the metal combustion chamber wall in experiment 3, it appears that the spray rebounds off the wall, but this is not conclusive. In contrast, experiment 7 (which also uses open-valve injection) does show a significant impingement pattern on the combustion chamber wall.

4.4.2 Film flow atomization

When a significant quantity of liquid fuel is present on the head, it can be forced into the valve gap by recirculating flow in the combustion chamber. This film will then be torn apart by the intake flow and converted into droplets. This phenomenon was observed in experiment 2 with the injector that provided minimal atomization and in experiment 8. It is shown in Figure 4.26 and Figure 4.27.

4.4.3 Intake jet atomization

When a liquid fuel film is present on the head, it can be strip atomized by the intake flow. This phenomenon was only observed with the 2 mm valve lift. With 2 mm lift the intake flow is much closer to the head than with 6 mm lift. It is most clearly observed in experiment 4, as depicted in Figure 4.28.

4.4.4 IVO valve gap splashing

Whenever there is no backflow or very brief backflow, any liquid fuel film that was covering the intake valve gap can be expelled outward as the valve opens as shown in Figure 4.29. This phenomenon was observed in both experiments 5 and 8. It is shown in Figure 4.30 for experiment 5. Interestingly, the droplets created from this mechanism appear to move away from the valve and across its centerline in an asymmetrical fashion.

4.5 Temperature effects

In order to examine the effects of intake valve temperature, experiment 1 was repeated with a hotter intake valve as experiment 6. (See Figure 4.1 and Figure 4.6). The overall amount of fuel present is affected by the valve temperature, but the physical processes the fuel undergoes is not. On a crank angle basis, the mixture preparation mechanisms were identical in both experiments, although the relative amounts of fuel present due to each mechanism were not.

Engine speed	1000 RPM
Fuel	Indolene, grade UTG-96
Equivalence ratio	Stoichiometric, $\phi \approx 1 \pm 0.03$
Volumetric efficiency *(based on ambient air density)*	≈ 26 % *

Table 4-1: Fixed operating conditions for the experiments

** Note: This corresponds to 0.4 bar intake pressure at 6mm lift and the intermediate valve timing. All other experiments were matched to the airflow rate at this condition.*

Experiment #	Injector	SOI	Lift	IVO	Tvalve
1	4-hole	Closed-valve	6 mm	5° bTC	25 °C
2	1-hole	Closed-valve	6 mm	5° bTC	25 °C
3	4-hole	Open-valve	6 mm	5° bTC	25 °C
4	4-hole	Closed-valve	2 mm	5° bTC	25 °C
5	4-hole	Closed-valve	6 mm	25° aTC	25 °C
6	4-hole	Closed-valve	6 mm	5° bTC	50 °C
7	4-hole	Open-valve	2 mm	5° bTC	25 °C
8	4-hole	Closed-valve	2 mm	25° aTC	25 °C

Table 4-2: Operating conditions for the experiments

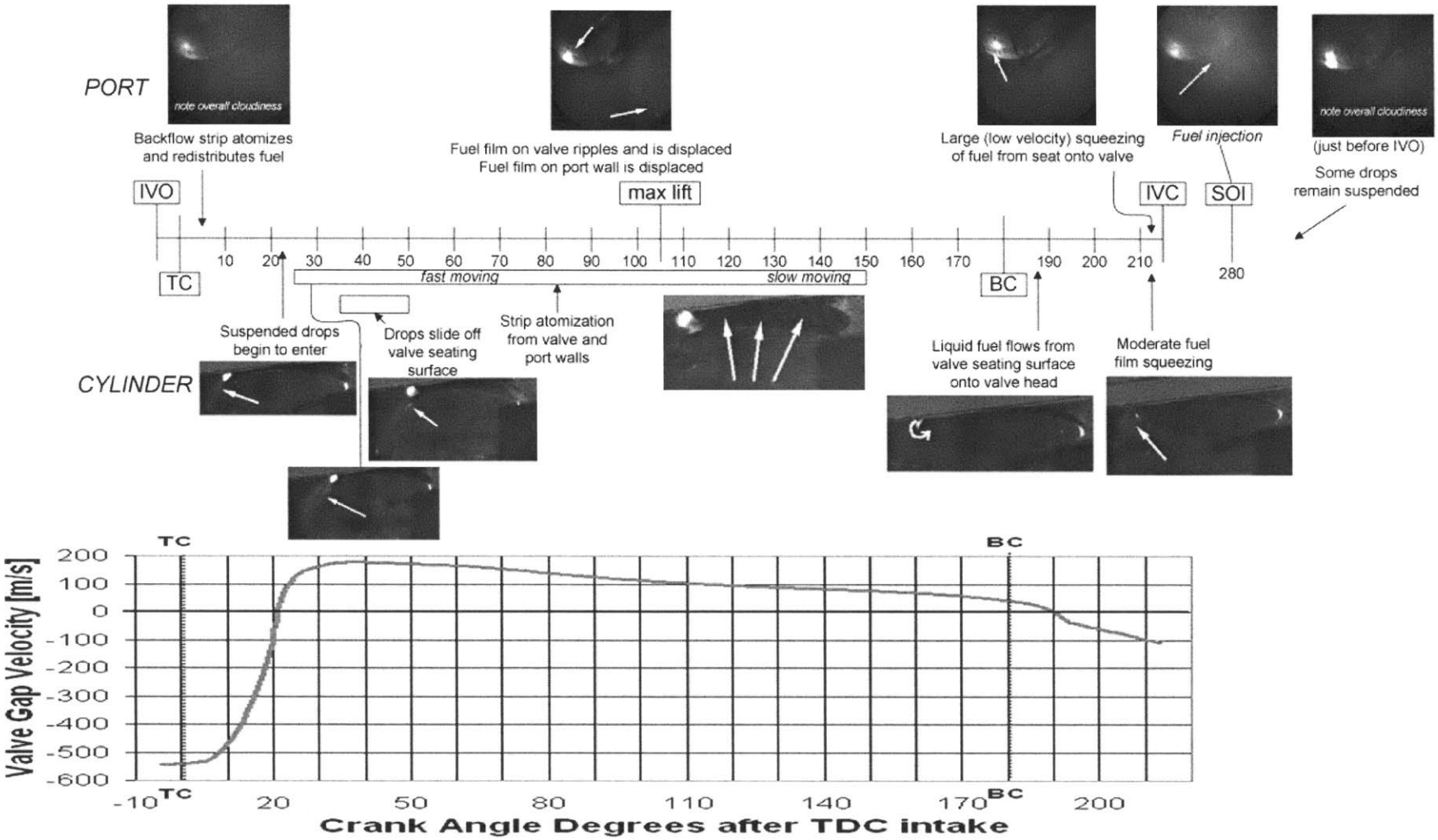

Figure 4.1: Event diagram for experiment 1

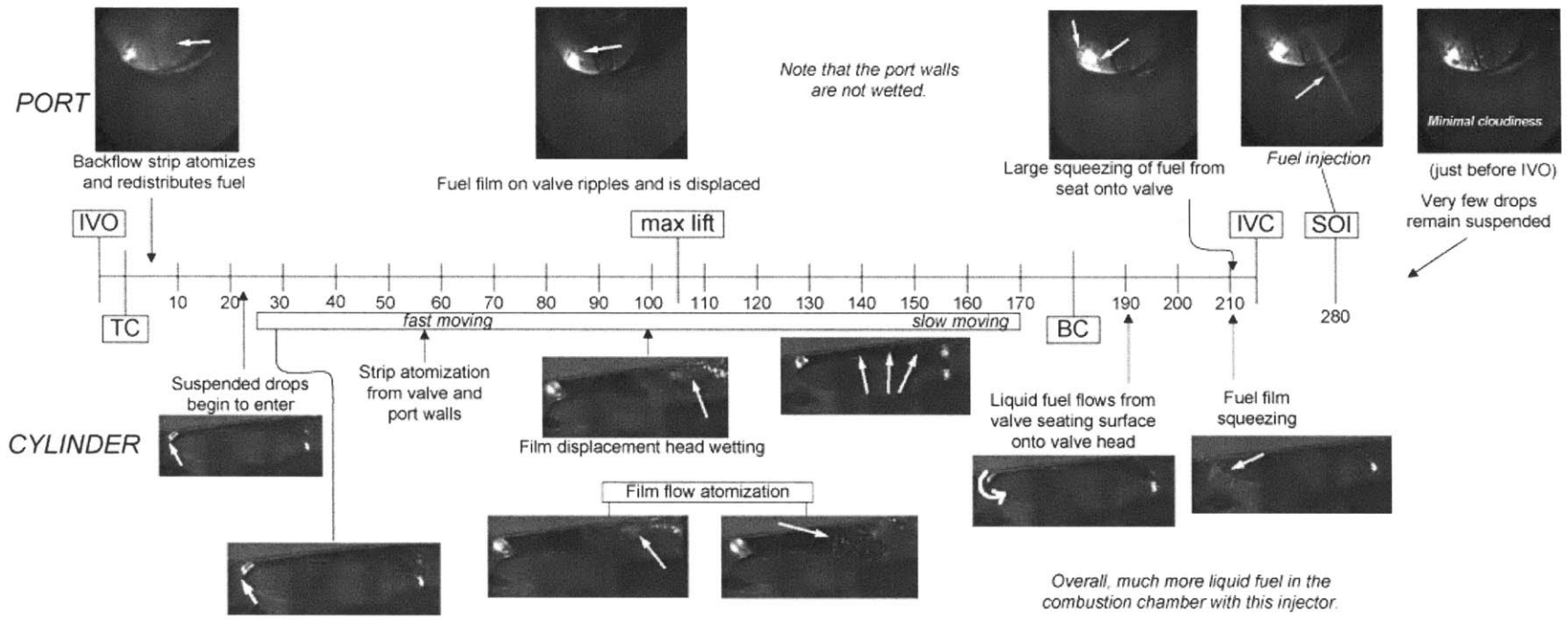

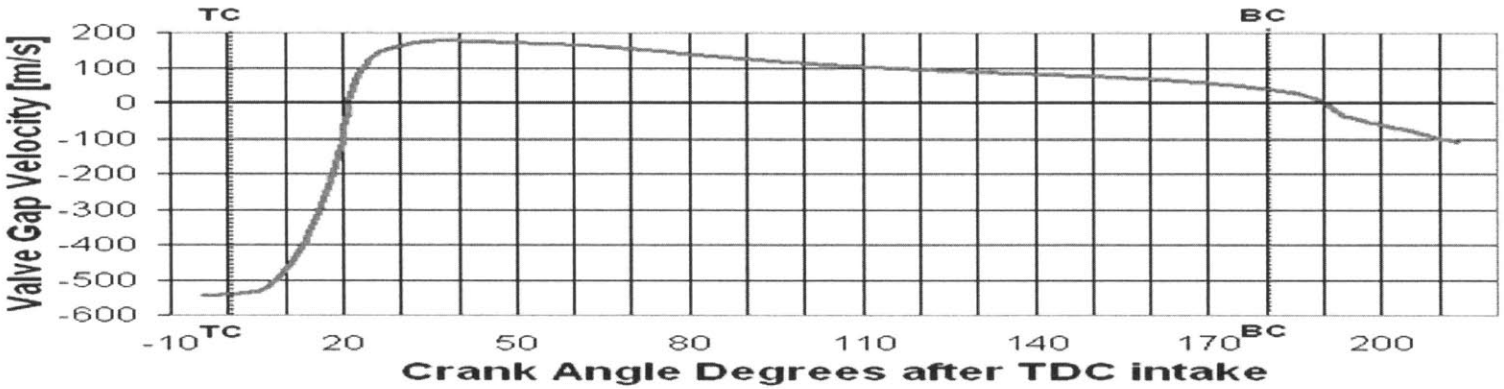

Figure 4.2: Event diagram for experiment 2

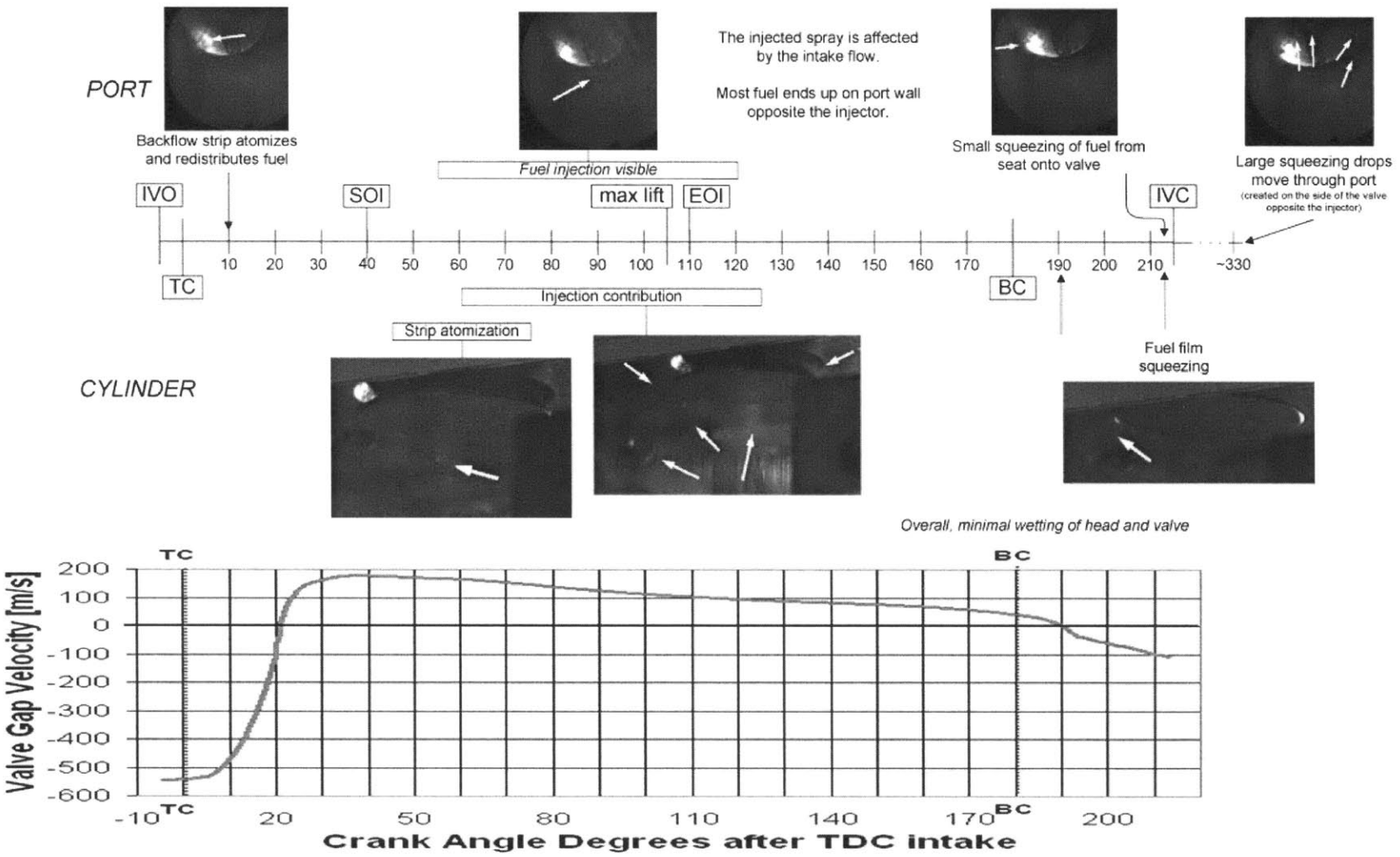

Figure 4.3: Event diagram for experiment 3

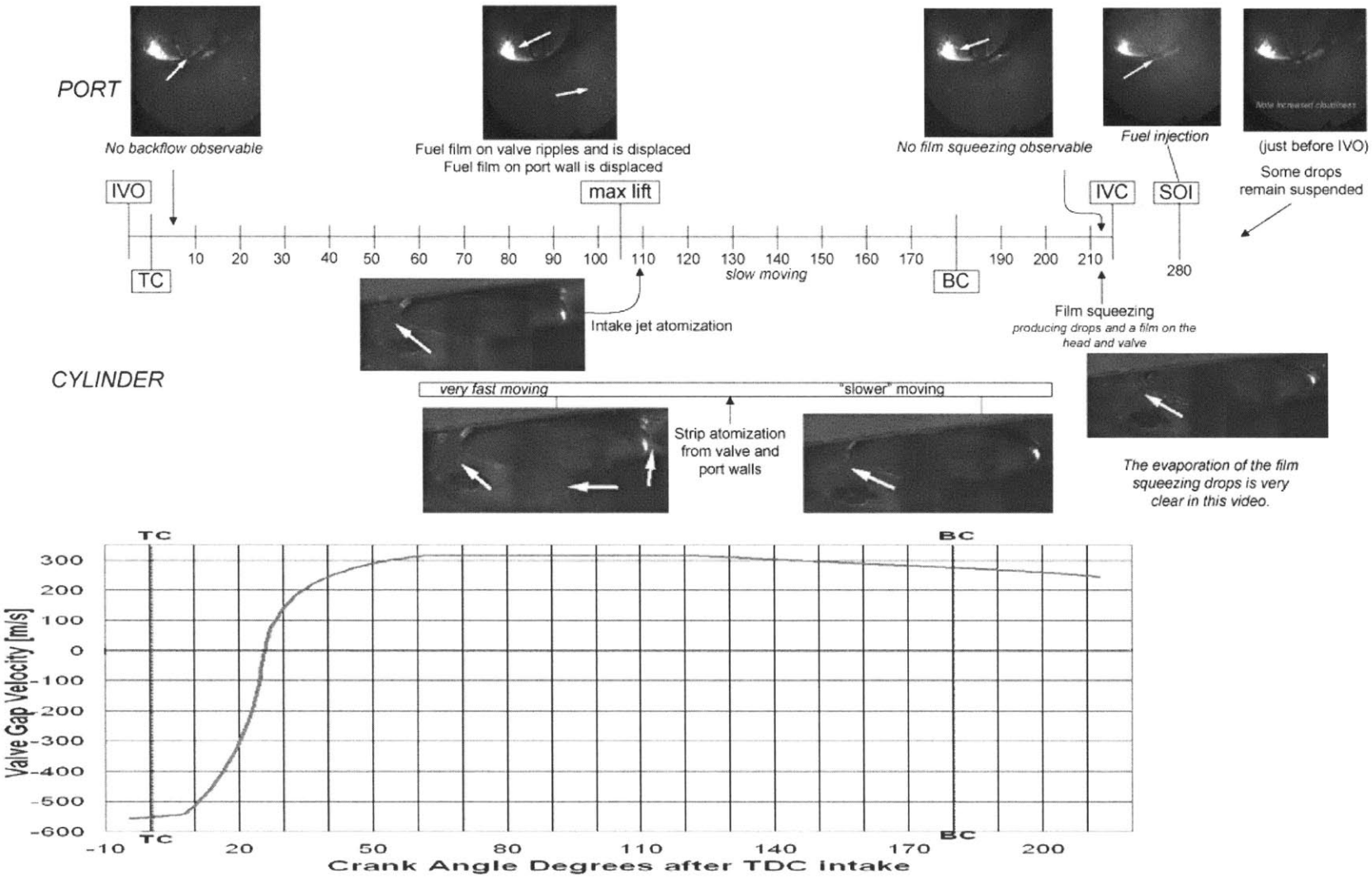

Figure 4.4: Event diagram for experiment 4

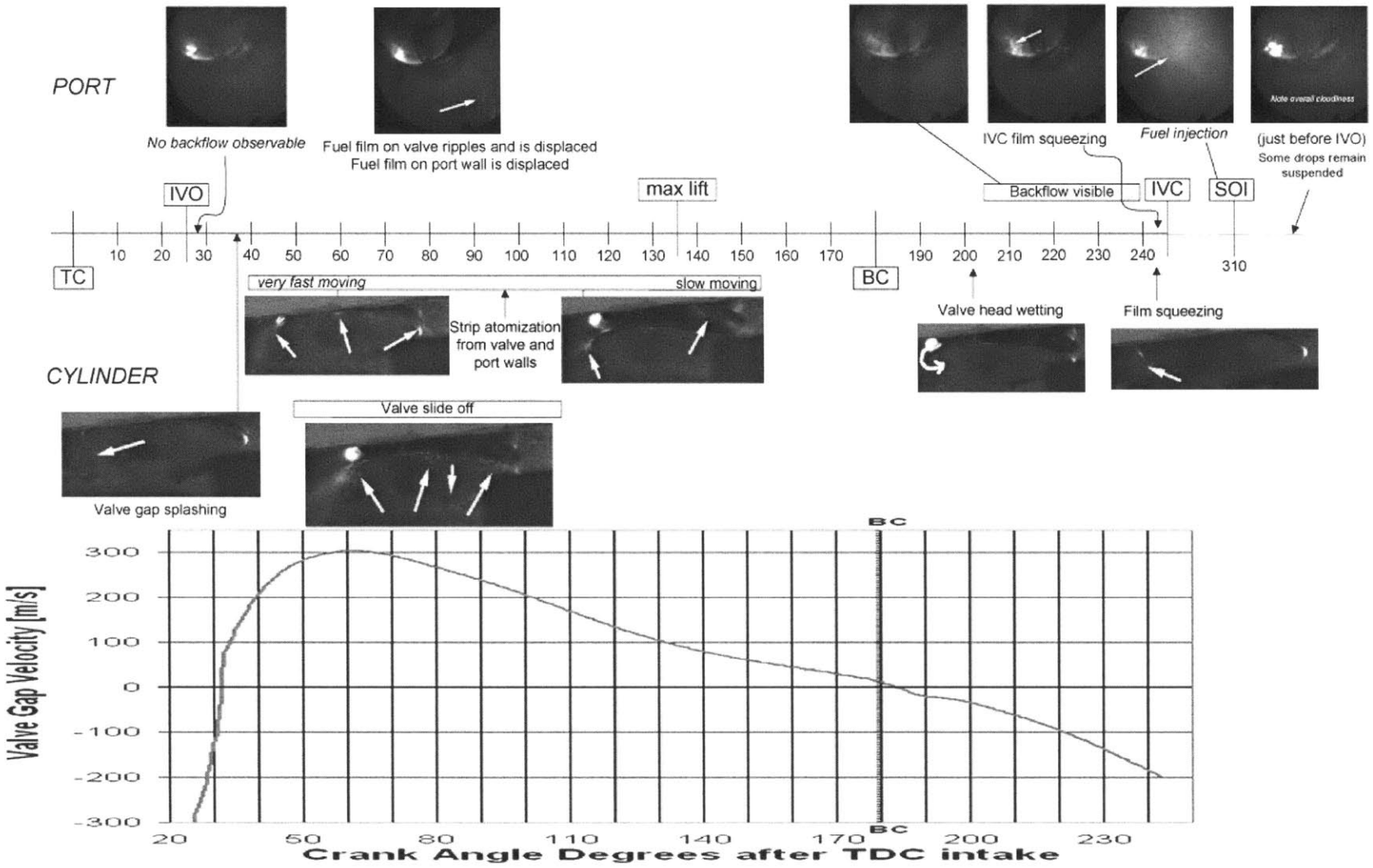

Figure 4.5: Event diagram for experiment 5

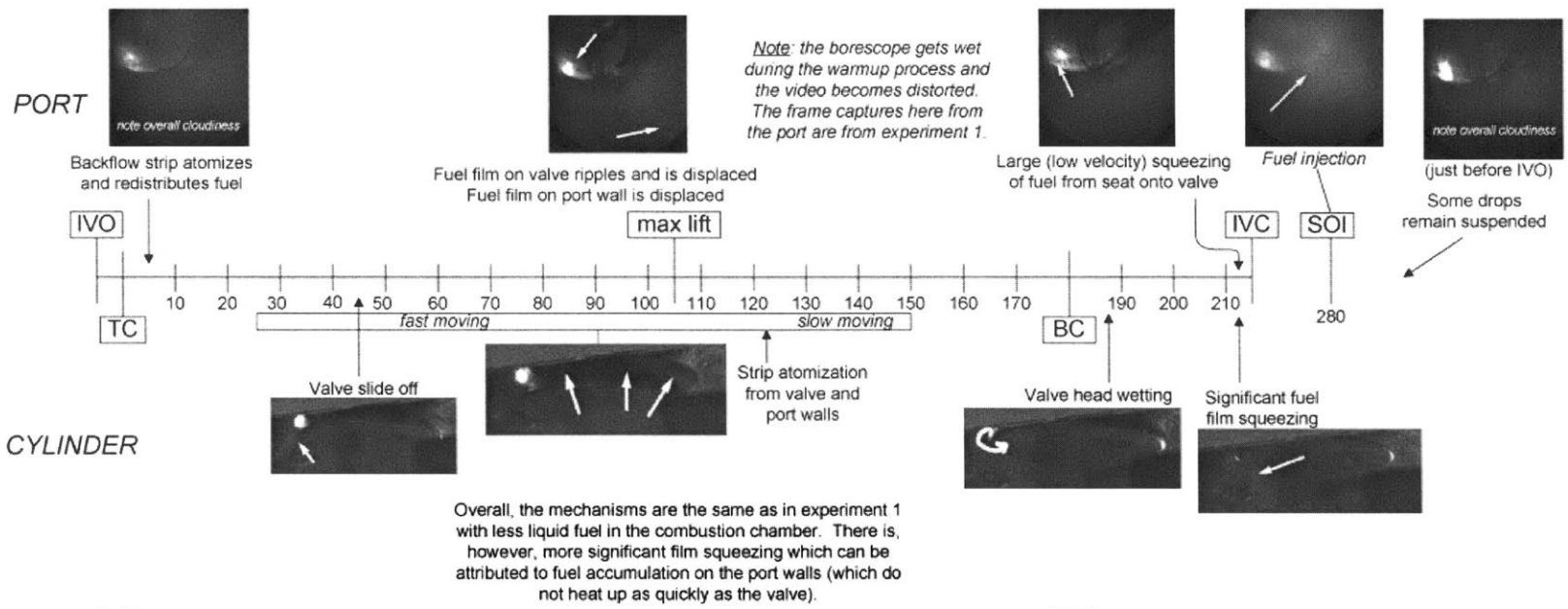

Overall, the mechanisms are the same as in experiment 1 with less liquid fuel in the combustion chamber. There is, however, more significant film squeezing which can be attributed to fuel accumulation on the port walls (which do not heat up as quickly as the valve).

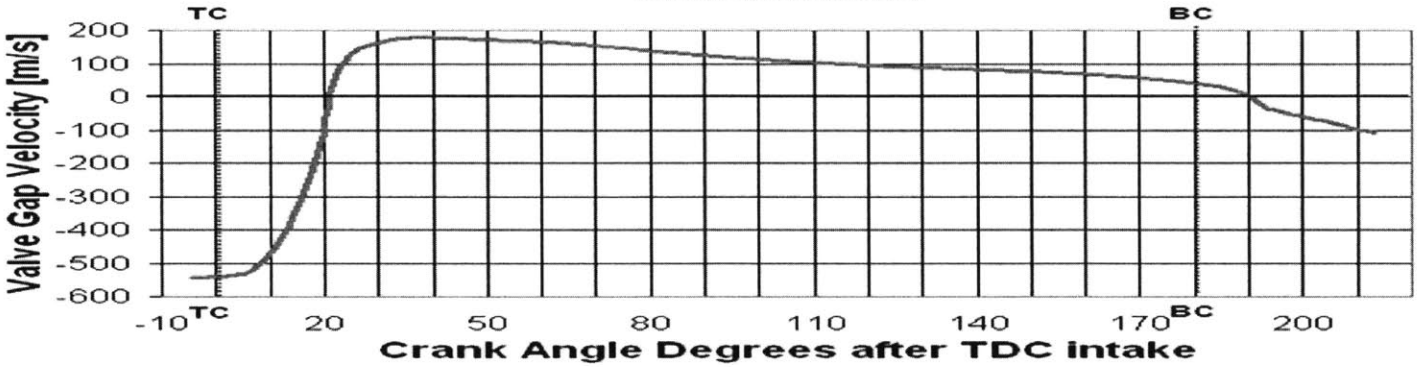

Figure 4.6: Event diagram for experiment 6

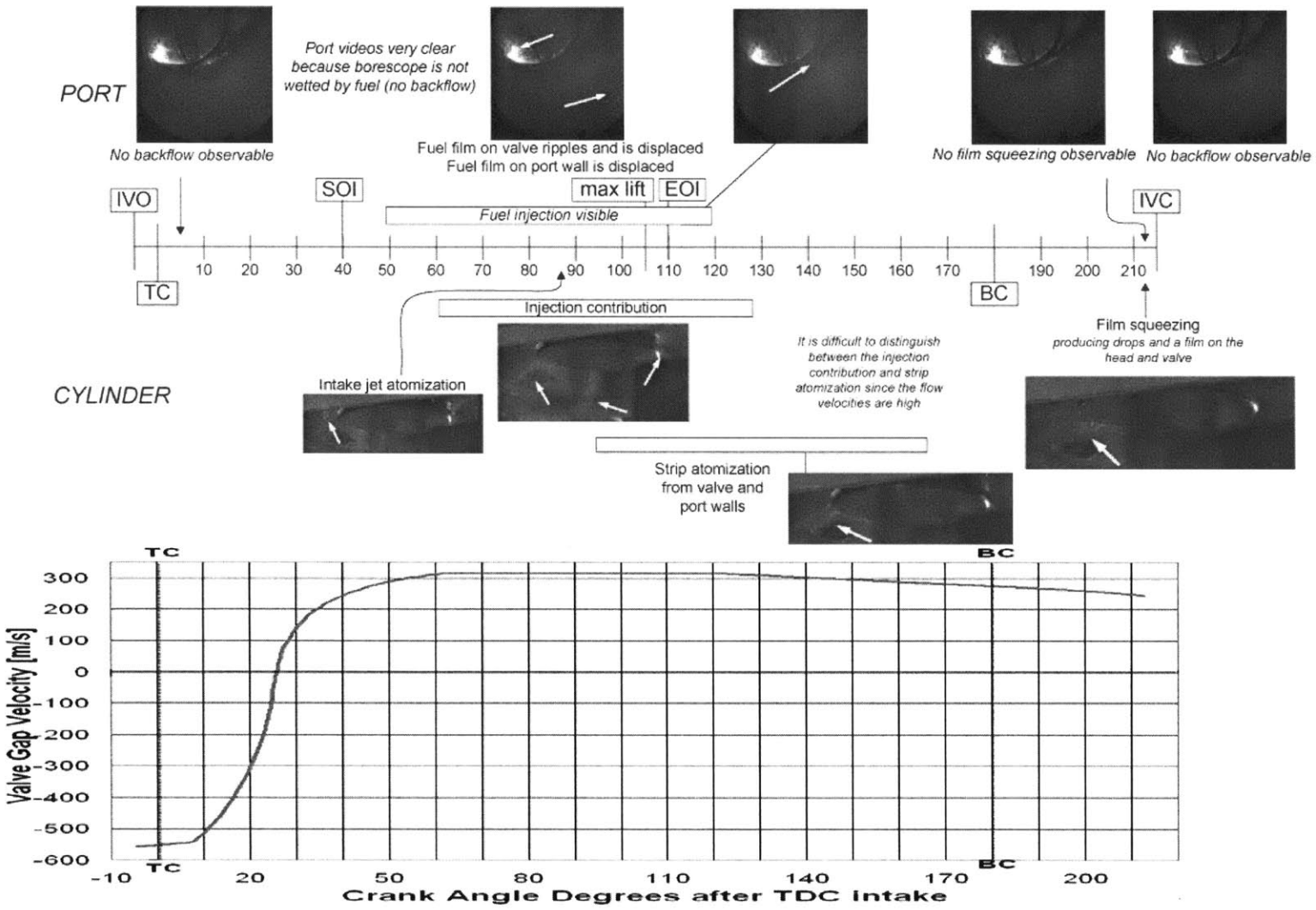

Figure 4.7: Event diagram for experiment 7

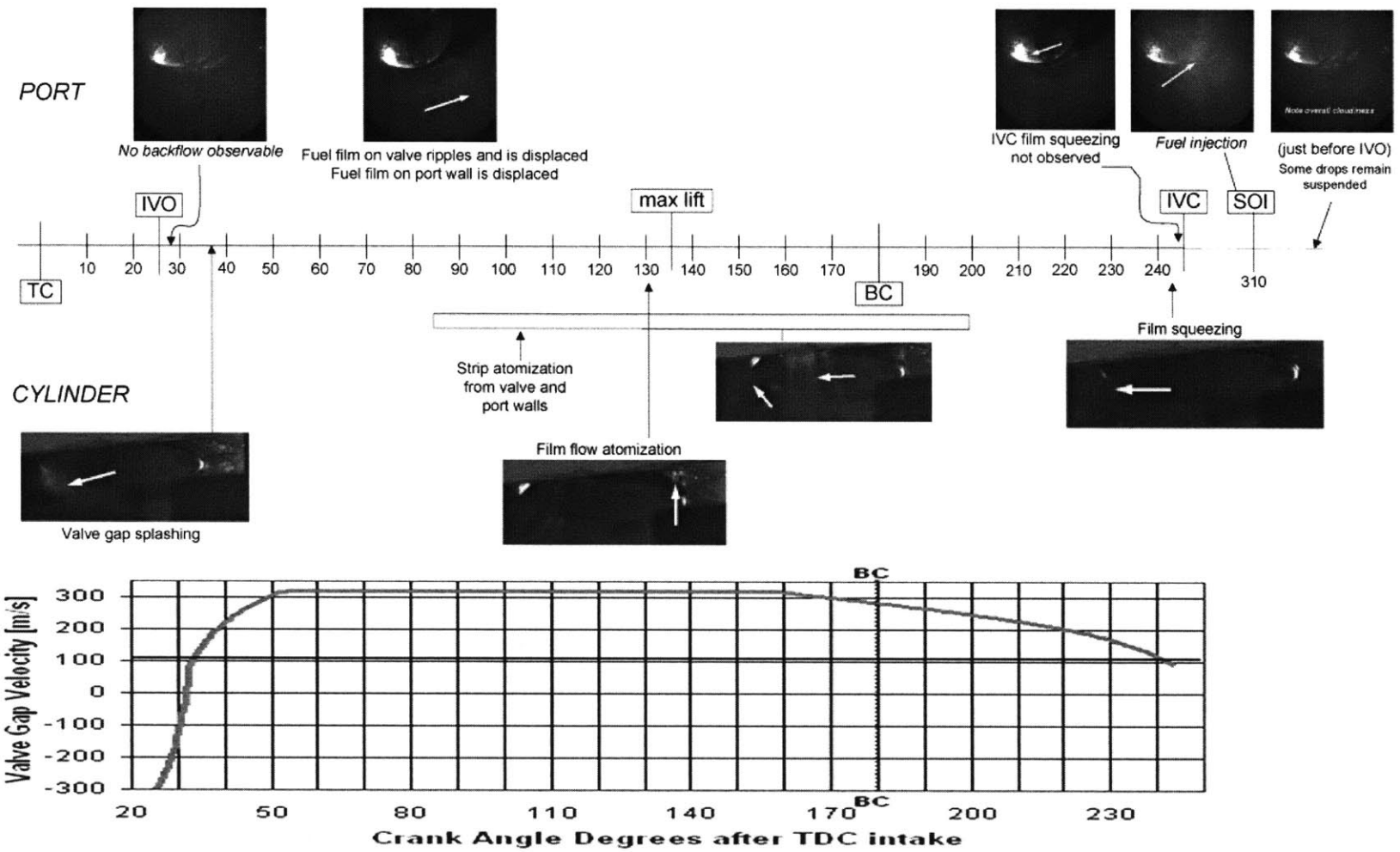

Figure 4.8: Event diagram for experiment 8

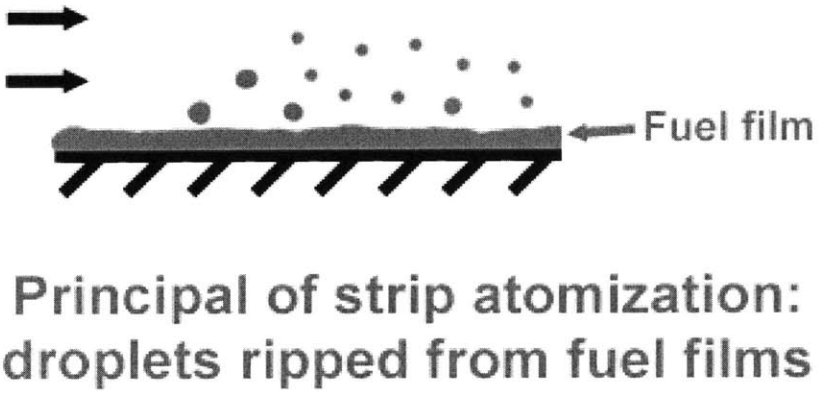

Figure 4.9: Strip atomization

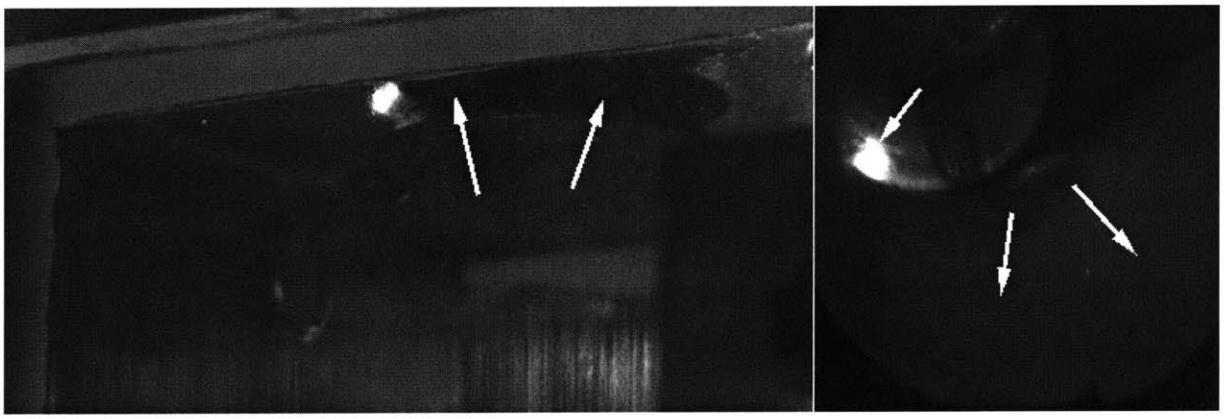

Figure 4.10: Evidence of strip atomization during forward flow, frames taken from video 1

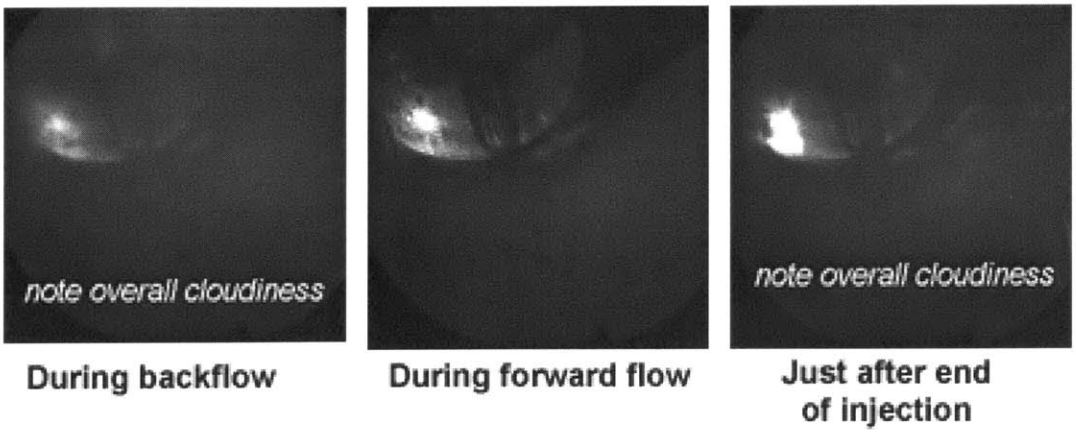

Figure 4.11: Evidence of strip atomization during intake valve opening backflow, frames taken from video 1.

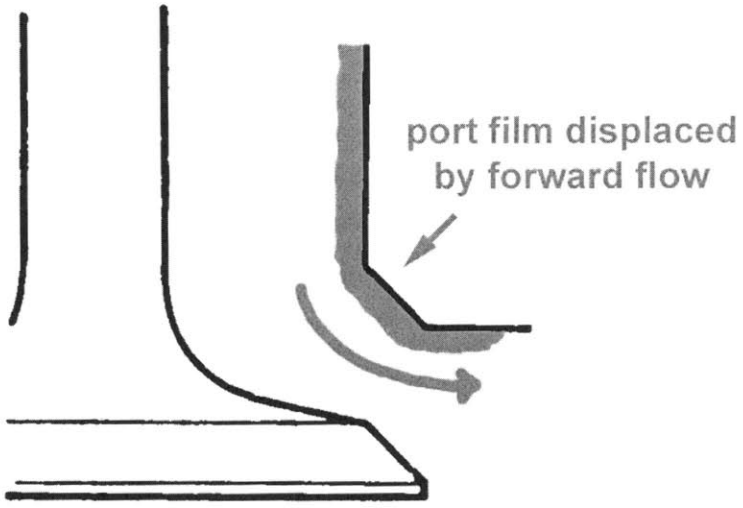

Figure 4.12: Film displacement head wetting

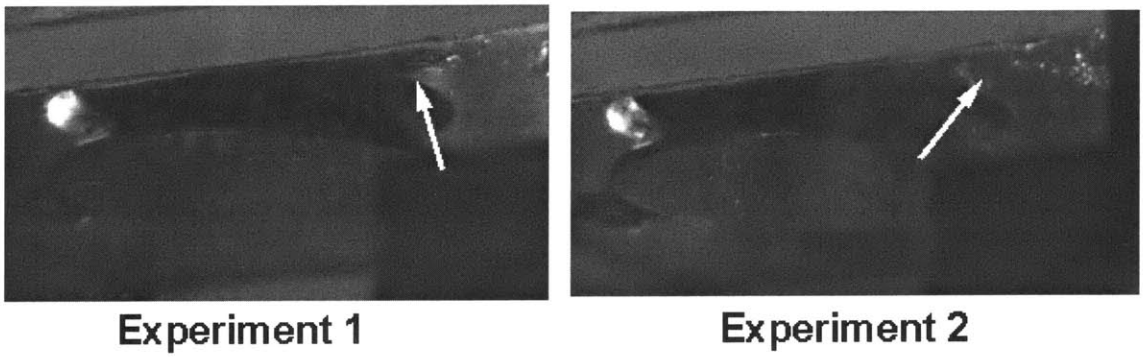

Figure 4.13: Evidence of film displacement head wetting.
Frame from experiment 1 is roughly 130 CAD aTDC-intake while the frame from experiment 2 is roughly 100 CAD aTDC-intake.

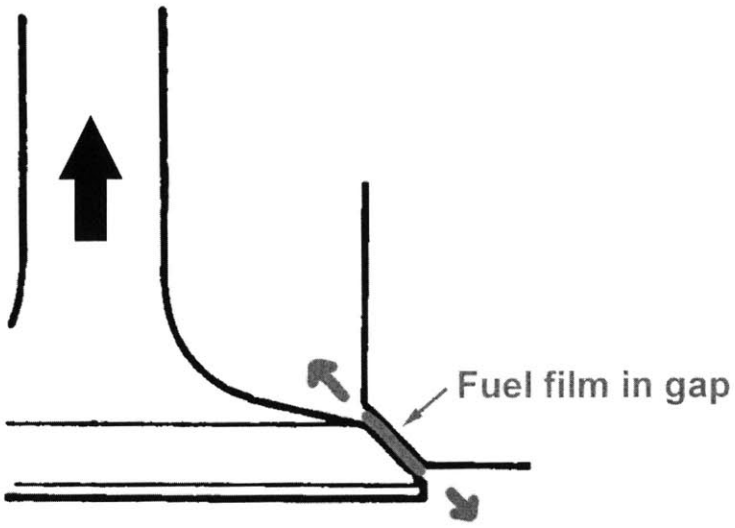

Figure 4.14: IVC film squeezing

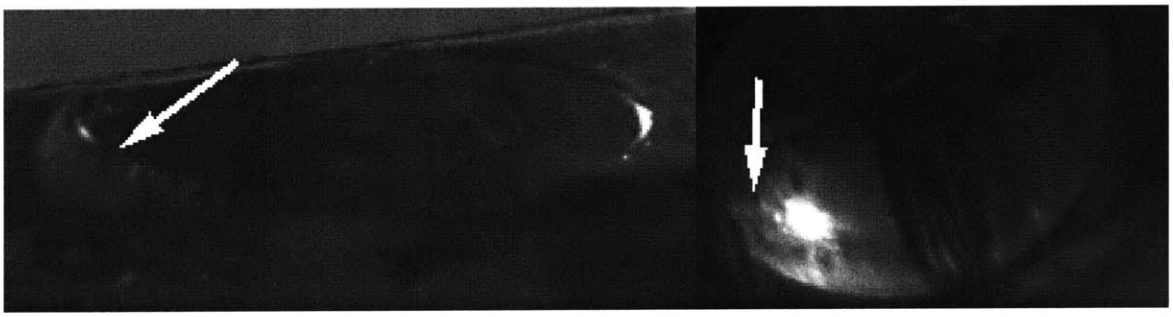

Figure 4.15: Film squeezing in experiment 1.

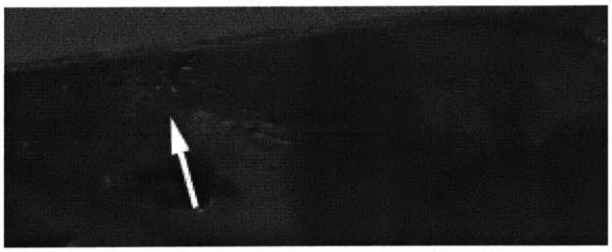

Experiment 4

Experiment 7

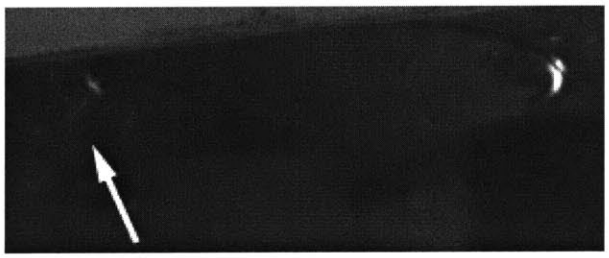

Experiment 8

Figure 4.16: Evidence of film squeezing being affected by intake flow

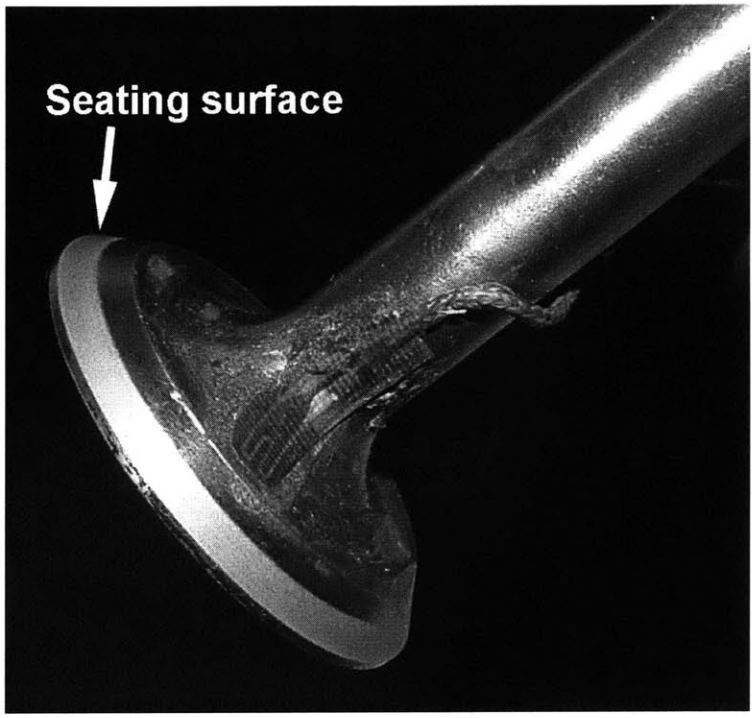

Figure 4.17: Valve seating surface

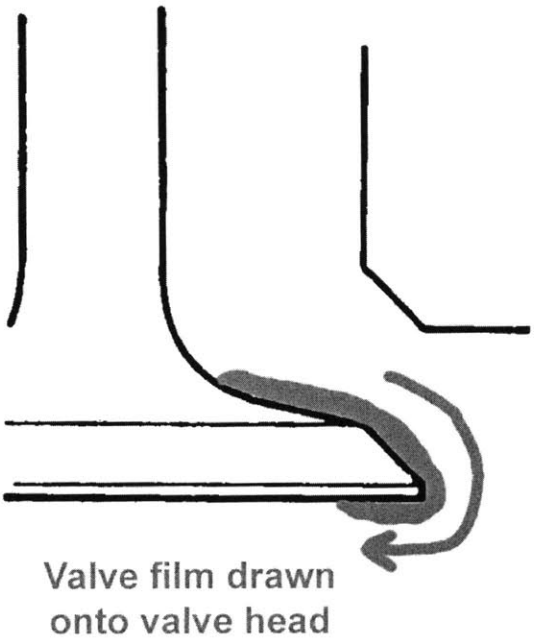

Figure 4.18: Valve head wetting

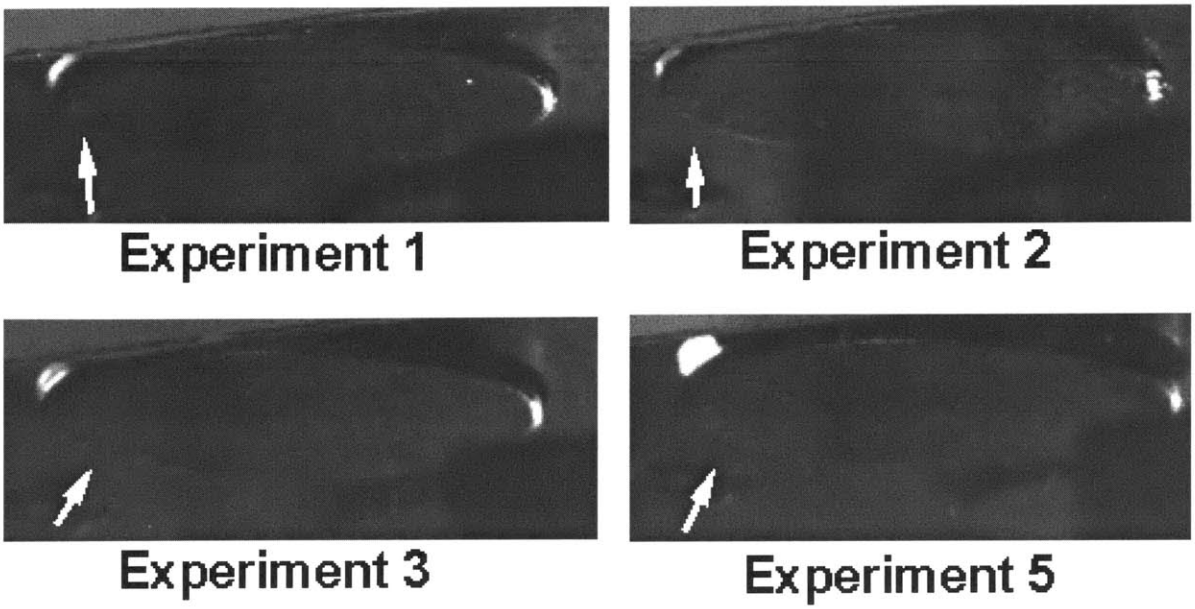

Figure 4.19: Valve head wetting in experiments 1, 2, 3, and 5.

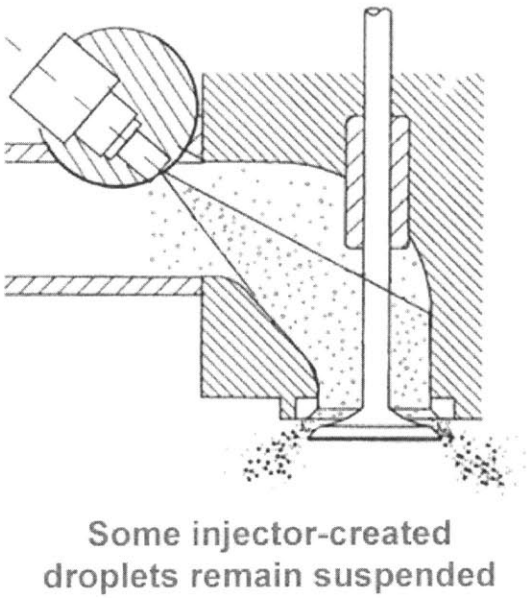

Figure 4.20: Injection contribution

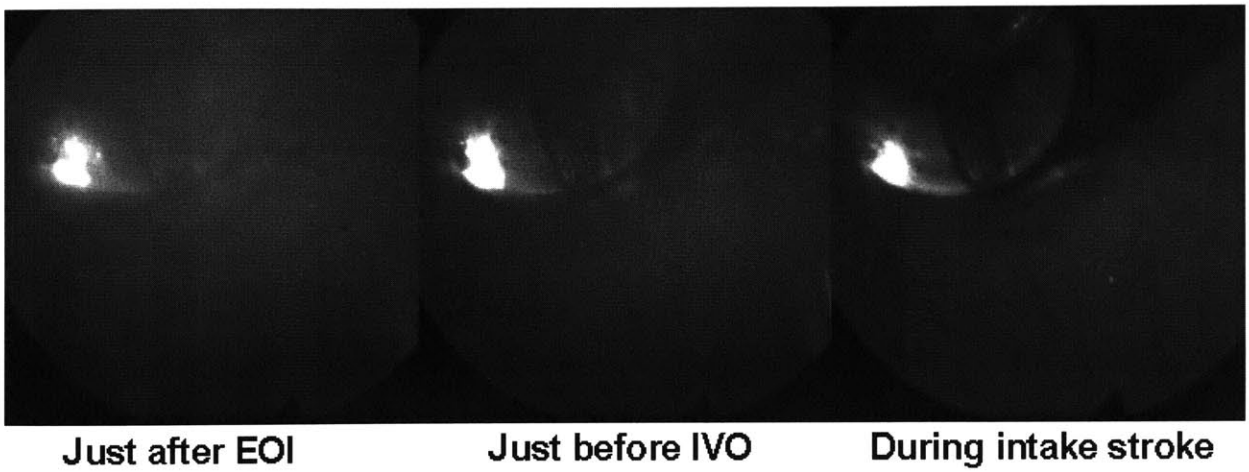

Figure 4.21: The persistence of injector generated droplets in the intake port with closed-valve injection, experiment 1.

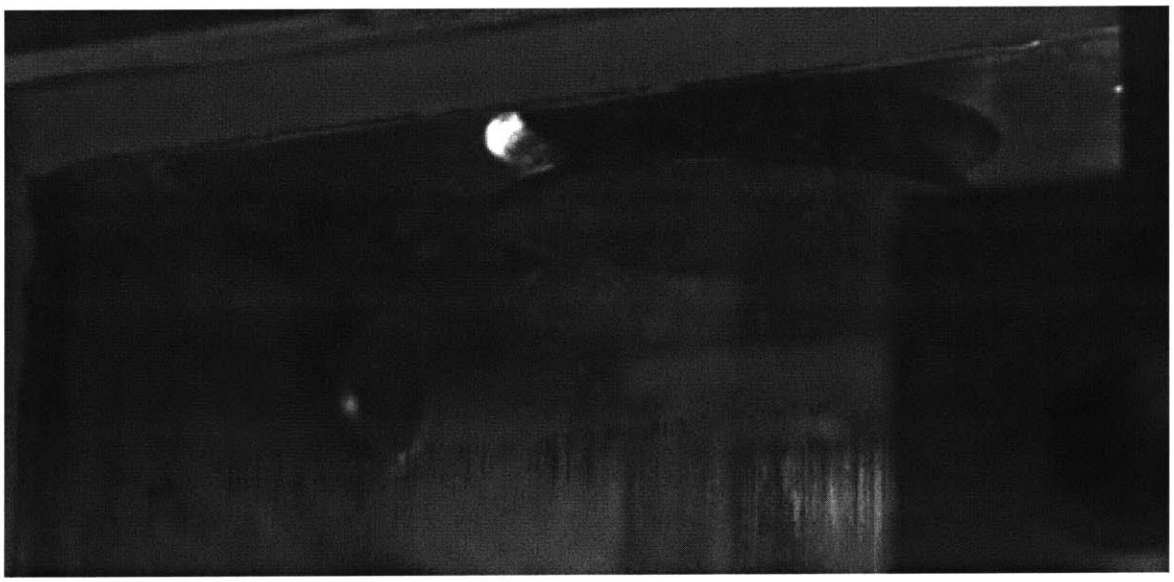

Figure 4.22: Open-valve injection, experiment 3.

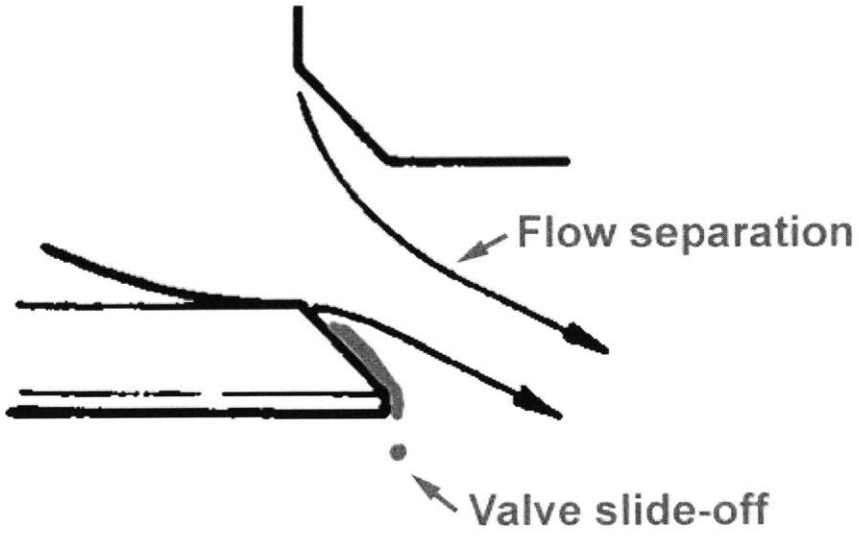

Figure 4.23: Valve slide-off

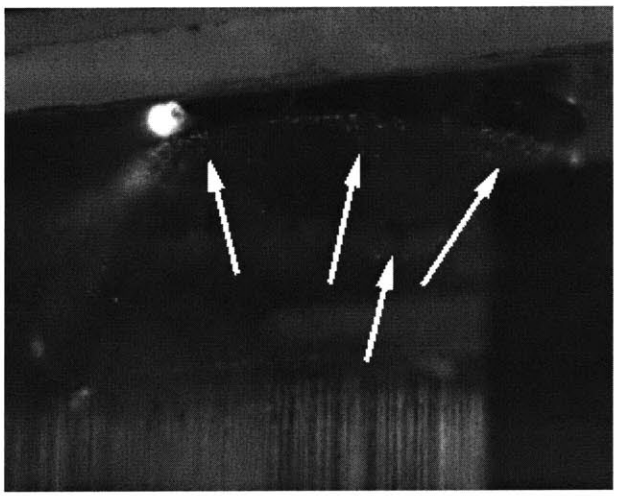

Figure 4.24: Valve slide-off in experiment 5.

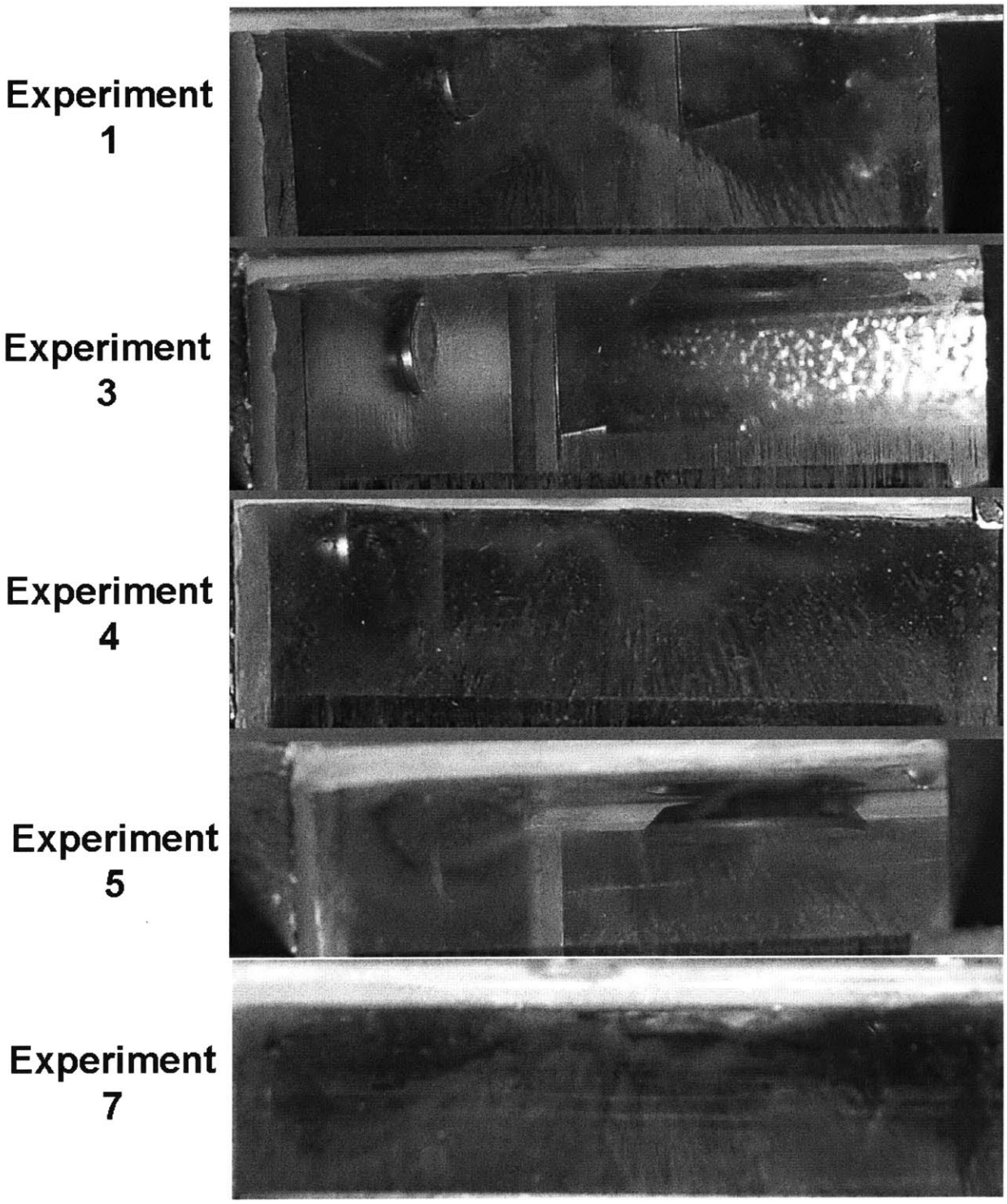

Figure 4.25: Impingement patterns left on combustion chamber windows for selected experiments.

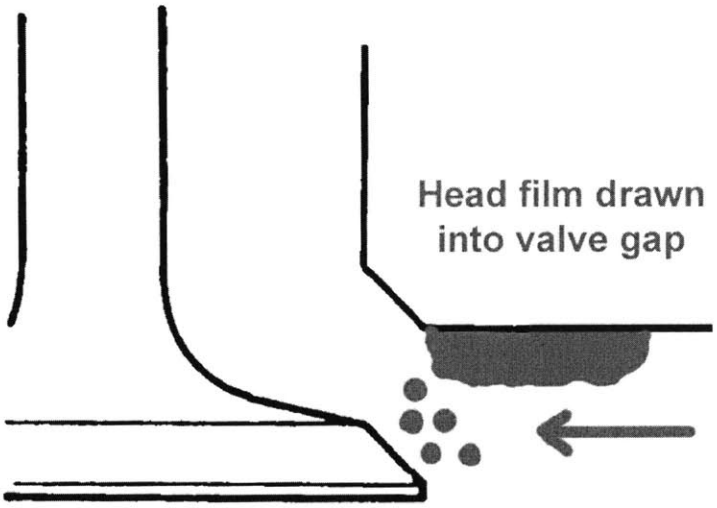

Figure 4.26: Film flow atomization

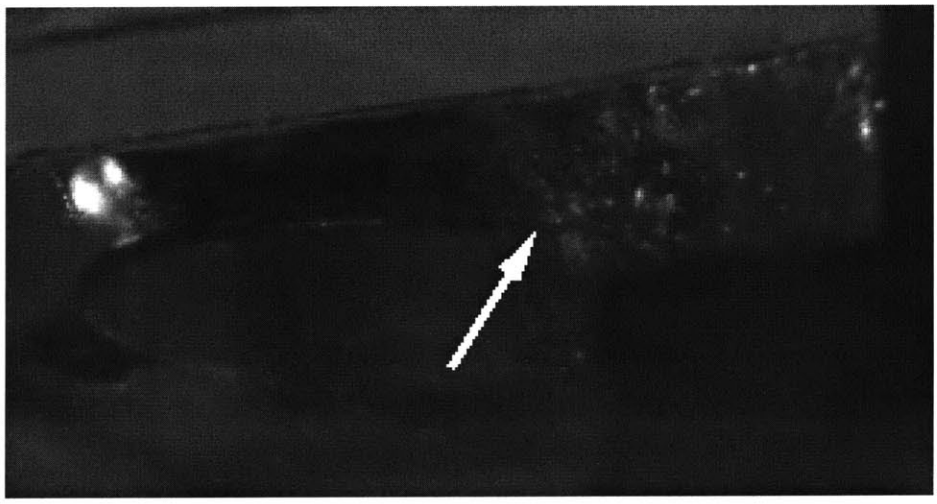

Figure 4.27: Film flow atomization, experiment 2.

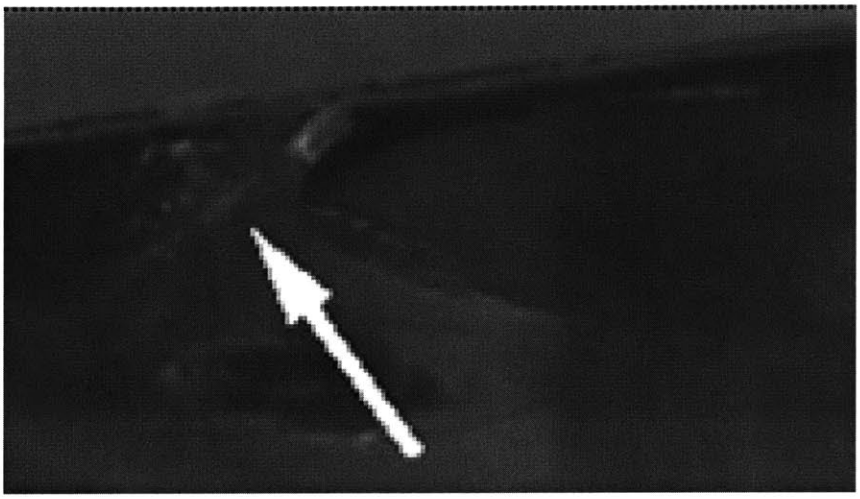

Figure 4.28: Intake jet atomization, experiment 4.

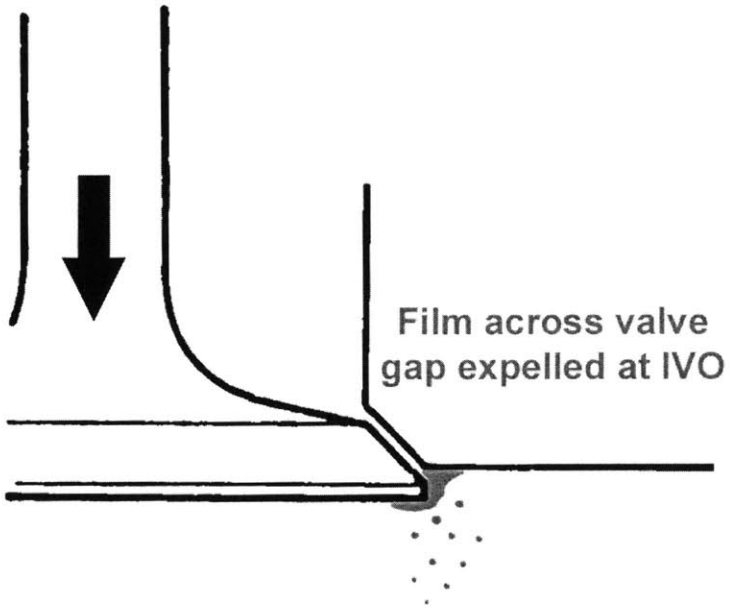

Figure 4.29: IVO valve gap splashing

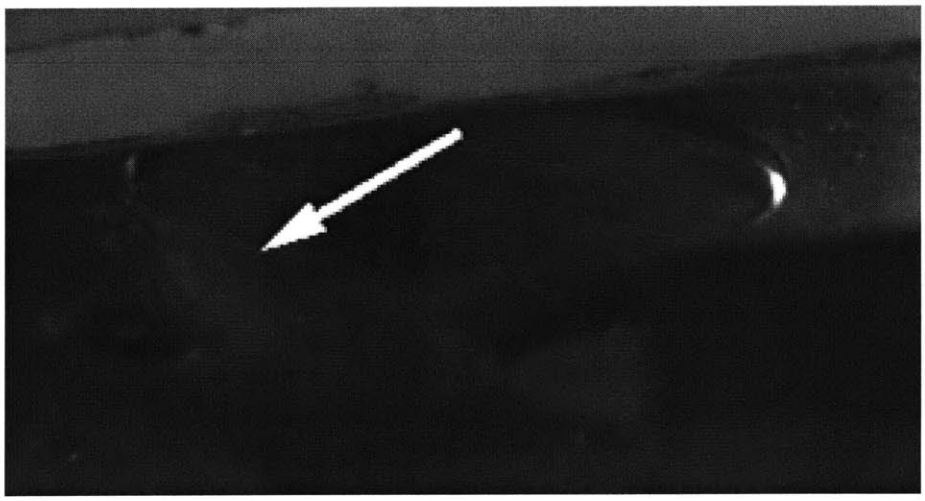

Figure 4.30: Valve gap splashing, experiment 5

5 Summary and Conclusions

Both liquid fuel transport and in-cylinder conversion mechanisms for droplets and films were identified in this study, along with the conditions that create them. They are summarized in Table 5-1. The mechanisms that transport liquid fuel into the combustion chamber include strip atomization, film displacement head wetting, IVC seat film squeezing, valve head wetting, injection contribution, and valve slide-off. The in-cylinder conversion mechanisms include coalescence on combustion chamber walls, film flow atomization, intake jet atomization, and IVO valve gap splashing.

Unfortunately, the idea that higher flow velocities and thus higher shear rates will result in improved mixture preparation is somewhat oversimplified. There are complex interactions that occur and larger flow velocities can actually be detrimental to mixture preparation. For example, a larger quantity of fuel can impinge upon the combustion chamber wall or increased valve slide-off can occur resulting in less kinetic energy imparted to the fuel droplets. Furthermore, if retarded intake valve opening is used to obtain larger flow velocities, any benefits from the backflow at intake valve opening can be lost. In short, higher flow velocities can be both beneficial and detrimental.

Mechanism	Description
TRANSPORT MECHANISMS	
Strip atomization 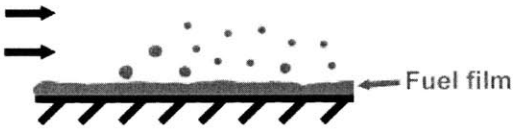	Droplets are ripped from fuel films by high velocity airflow, or are formed by film breakup
Film displacement head wetting 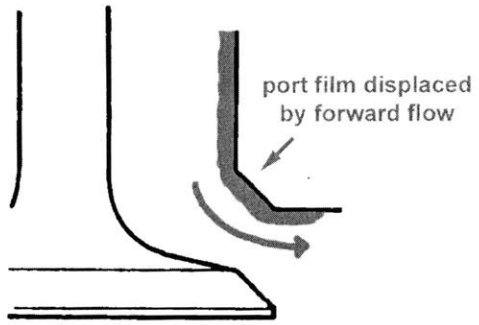	Low velocity inflow displaces film onto head, where it remains as a film due to surface tension.
IVC seat film squeezing 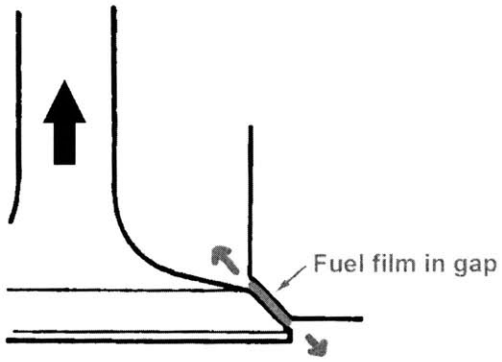	Liquid fuel in the valve seat is squeezed into the port and combustion chamber at intake valve closing, as either drops or a film.
Valve head wetting 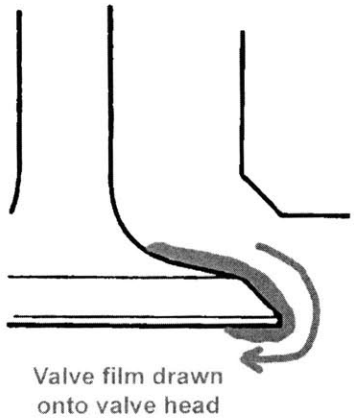	Low velocity inflow allows a film on the valve to be drawn onto the valve head by gravity, where it remains as a film due to surface tension.
Injection contribution	Even with closed-valve injection, some of the

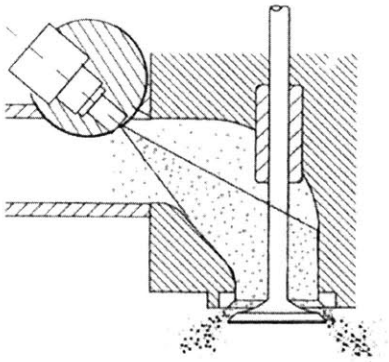	droplets created by the fuel injector remain suspended in the intake port.
Valve slide-off 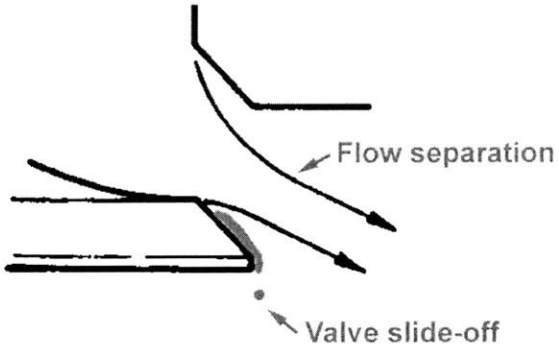	High velocity inflow through a sufficiently open valve results in flow separation, which causes any fuel on the valve seating surface to be drawn into the combustion chamber due to gravity.
CONVERSION MECHANISMS	
Drop coalescence	Droplets that enter the combustion chamber coalesce to form films on the combustion chamber walls.
Film flow atomization 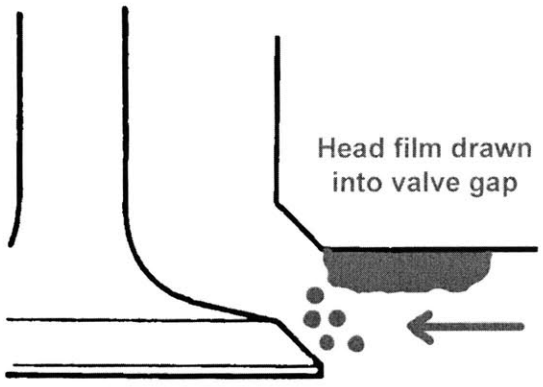	A liquid fuel film on the head is drawn into the valve gap where it is torn into droplets.
Intake jet atomization	Typically with low lift, the intake flow can strip atomize a fuel film present on the head.
IVO valve gap splashing	When there is no or very brief backflow, any liquid fuel covering the valve gap is expelled outward when the valve opens.

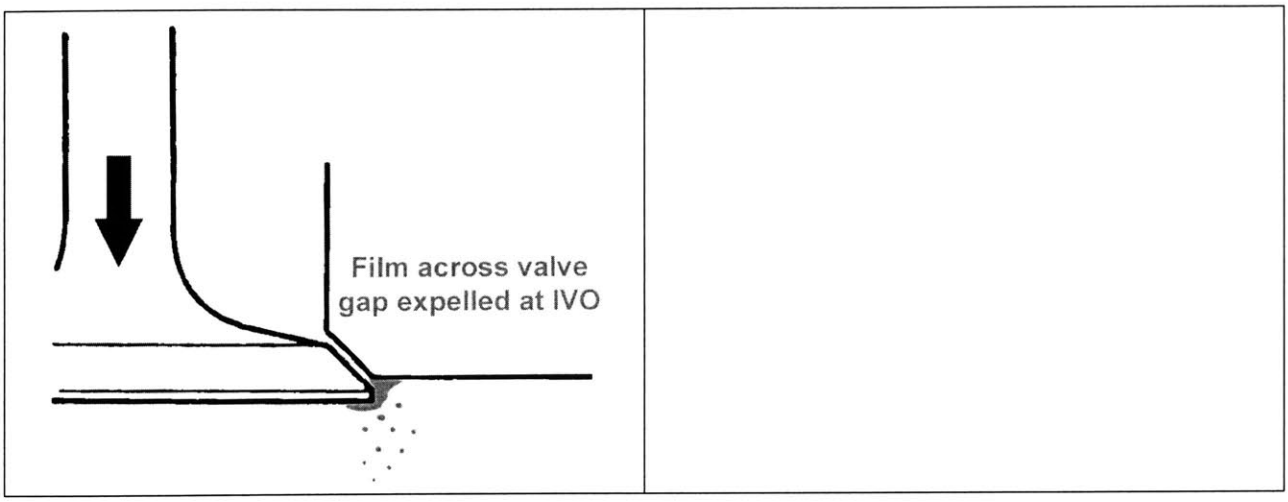

Table 5-1: Summary of mixture preparation mechanisms

REFERENCES

[1] Heywood, J.B. *Internal Combustion Engine Fundamentals*. New York: McGraw-Hill, 1988.

[2] Stanglmaier, R.H., Hall, M.J., and Matthews, R.D. "In-Cylinder Fuel Transport During the First Cranking Cycles in a Port Injected 4-Valve Engine." *SAE Paper 970043*, 1997.

[3] Zhang, Y. and Cheng, W. "Fuel sulfur and aging effects on the oxygen storage capacity in three way catalytic converters." *SAE Paper 2003-01-1874*, 2003.

[4] Alkidas, A.C. "Intake-Valve Temperature and the Factors Affecting It." *SAE Paper 971729*, 1997.

[5] Santoso, H. and Cheng, W.K. "Mixture preparation and hydrocarbon emissions behaviors in the first cycle of SI engine cranking." *SAE Paper 2002-01-2805*, 2002.

[6] Liebl, J., et al. "The New BMW 4-Cylinder Engine with Valvetronic. Part Two: Thermodynamics and Functional Features." *Motortechnische Zeitschrift*, MTZ 62 7/8, 2001.

[7] Nagumo, S. and Hara, S. "Study of Fuel Economy Improvement through Control of Intake Valve Closing Timing: Cause of Combustion Deterioration and Improvement." *JSAE Review 16*, 1995. pp. 13-19.

[8] Takemura, S. et al. "A Study of a Continuous Variable Valve Event and Lift (VEL) System." *SAE Paper 2001-01-0243*, 2001.

[9] Flierl, R. and Klüting, M. "The Third Generation of Valvetrains – New Fully Variable Valvetrains for Throttle-Free Load Control." *SAE Paper 2000-01-1227*.

[10] Klein, F. et al. "The Influence of the Valve Stroke Design in Variable Valve Timing Systems on Load Cycle, Mixture Formation and the Combustion Process in Conjunction with Throttle-free Load Governing." *SAE Paper 981030*, 1998.

[11] Tuttle, J.H. "Controlling Engine Load by Means of Early Intake-Valve Closing." SAE Paper 820408, 1982.

[12] Hara, S., Nakajima, Y., Nagumo, S. "Effects of Intake Valve Closing Timing on Spark-Ignition Engine Combustion." *SAE Paper 850074*, 1985.

[13] Tuttle, J.H. "Controlling Engine Load by Means of Late Intake-Valve Closing." *SAE Paper 800794*, 1980.

[14] Urata, Y. et al. "A Study of Vehicle Equipped with Non-Throttling S.I. Engine with Early Intake Valve Closing Mechanism." *SAE Paper 930820*, 1993.

[15] Gottschalk, W. et al. "The Effect of the Intake Valve Lift of SI Engines on Mixture Formation, Fuel Consumption and Exhaust Emissions." *Motortechnische Zeitschrift*, MTZ 61 7/8, 2000.

[16] Shelby, M., Stein, R., and Warren, C. "A New Analysis Method for Accurate Accounting of IC Engine Pumping Work and Indicated Work." *SAE Paper 2004-01-1262*, 2004.

[17] Moriya, Y. et al. "A Newly Developed Intelligent Variable Valve Timing System – Continuously Controlled Cam Phasing as Applied to a New 3 Liter Inline 6 Engine." *SAE Paper 960579*, 1996.

[18] Shin, Y., Cheng, W.K., and Heywood, J.B. "Liquid Gasoline Behavior in the Engine Cylinder of a SI Engine." *SAE Paper 941872*, 1994.

[19] Meyer, R. and Heywood, J.B. "Liquid Fuel Transport Mechanisms into the Cylinder of a Firing Port-Injected SI Engine During Start Up." *SAE Paper 970865*, 1997.

[20] Meyer, R. "Liquid Fuel Transport into the Cylinder in Spark Ignition Engines." MIT PhD Thesis, 1998.

[21] Asmus, T.W. "Valve Events and Engine Operation." *SAE Paper 820749*, 1982.

[22] Giansetti, P. et al. "A Model for Residual Gas Fraction Prediction in Spark Ignition Engines." *SAE Paper 2002-01-1735*, 2002.

[23] Lefebvre, Arthur H. *Atomization and Sprays*. New York: Hemisphere, 1989.

[24] Pozar, M. Personal communication. March 15, 2004.

[25] Barbastathis, G. Personal communication. January 13, 2004.

Appendix 1: Valvetrain modifications and rocker arm design

For practical reasons the rocker ratio was varied to reduce the valve lift. This involved several modifications to the valvetrain as well as the design of new rocker arms.

One of the early decisions made in modifying the valvetrain was to design the rocker arms to utilize a common pushrod. A worksheet was constructed in Maple, a mathematics software package, to determine the required rocker arm geometry for each lift to ensure compatibility with the pushrod. Figure A1.1 shows a photograph of the new intake pushrod.

The existing lifter was made of steel and rode in a steel sleeve. Because longer rocker arms would cause a lateral force to be placed on the lifter, a new lifter was designed that was partially made of brass. The brass-steel combination is much less likely to bind under lateral loading. The portion of the lifter that contacted the cam lobes was still made of hardened steel. Figure A1.2 shows a photograph of the new lifter.

The desired intake valve lift dictated some of the new rocker arms' geometry. The remaining geometry was determined to satisfy three constraints. First, in order to avoid unexpected valvetrain dynamics, the new rocker arms could not exceed the rotational inertia of the existing arm. Second, due to the cyclic loading, the maximum stress in the new arms could not exceed the level present in the existing arm. Finally, in order to obtain true lift profiles and avoid valvetrain surging, the deflection of the new rocker arms under loading had to be negligible. Simultaneously satisfying these three constraints posed a significant challenge.

In order to accurately model the loading scenario, the response of the valve springs in the engine was determined. The spring constant was 346 lbf/in and the preload was 20 lbf compressive. The resulting maximum push rod force for each intake valve lift is given in Table A1.1. These are the design loads used in the subsequent analyses.

One half of the existing rocker arm (6.2 mm lift) was analyzed using the finite element software ABAQUS. Both the actual geometry and a pseudo geometry were analyzed. Figures XX and YY show the actual and pseudo geometry models. The pseudo geometry had the same cross-sectional area as the actual geometry at a given distance from the midplane, but assumed it was distributed symmetrically. The purpose in making this assumption is to enable elementary beam theory to be applied more easily (since locating the neutral axis becomes trivial).

Table A1.2 summarizes the results of this analysis. As can be seen, the pseudo geometry under predicts the maximum equivalent stress in the arm by a factor of $7.4/6.5 \approx 1.14$.

In order to design the new rocker arms, elementary beam theory was applied assuming a symmetric cross-section, as was done for the pseudo geometry. Based upon the above analysis and the assumption that geometries more "skewed" than the actual geometry from above would not be used, a factor of safety/uncertainty in the analysis method of 1.2 was used. Maple was used to carry out this analysis and verify the three design requirements.

The actual process of determining the new rocker arm designs was highly iterative. In the end, two rocker arms were designed: one for both 5 and 4 mm lift and one for both 3 and 2 mm lift. Figure A1. and Figure A1. show the final designs. The 5 and 4 mm rocker arm was able to satisfy the design requirements with a simple solid cross-section. The 3 and 2 mm arm, however, required an I-beam style cross-section.

It should be noted that it would have been extremely expensive to have these arms manufactured by a machine shop, as well as being very time-consuming and difficult to communicate the designs. The author of this thesis created the arms himself using CNC and conventional machine tools based on the output of the worksheets discussed above. It is for this reason that dimensioned engineering drawings of the arms are not available.

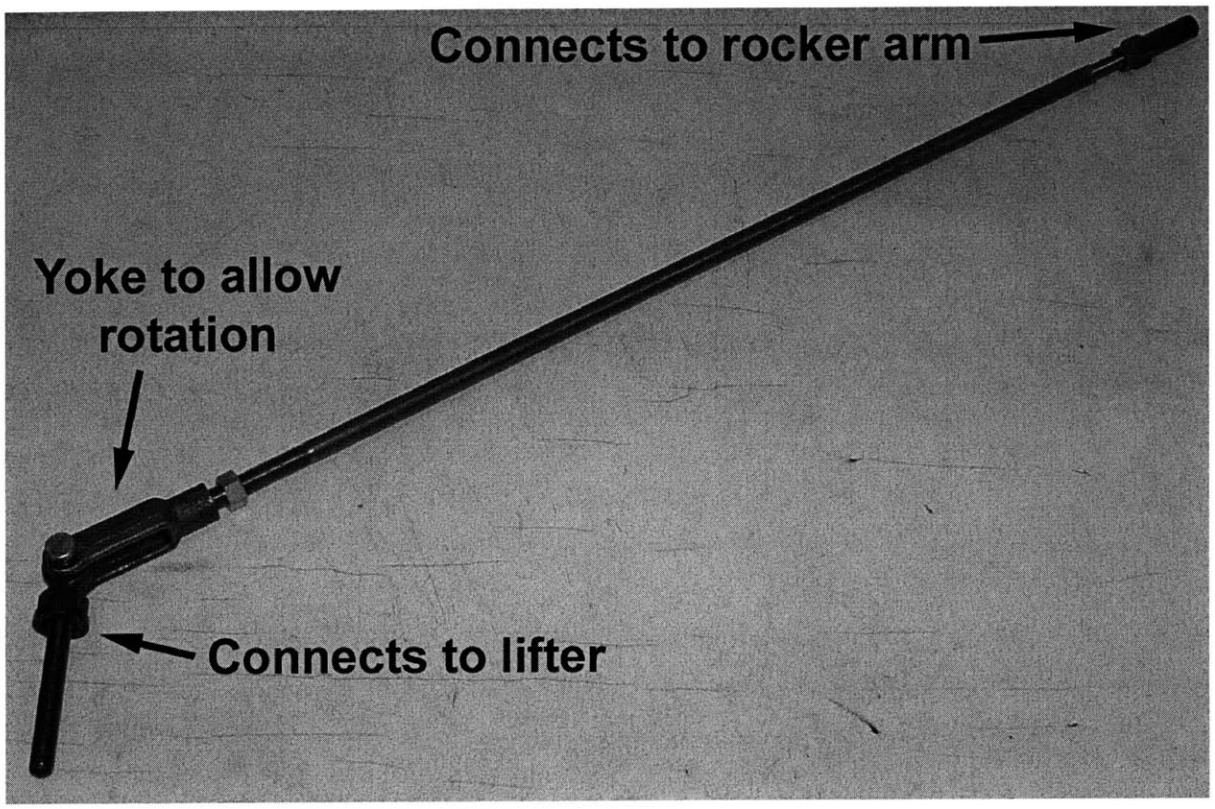

Figure A1.1: Photograph of the new intake pushrod

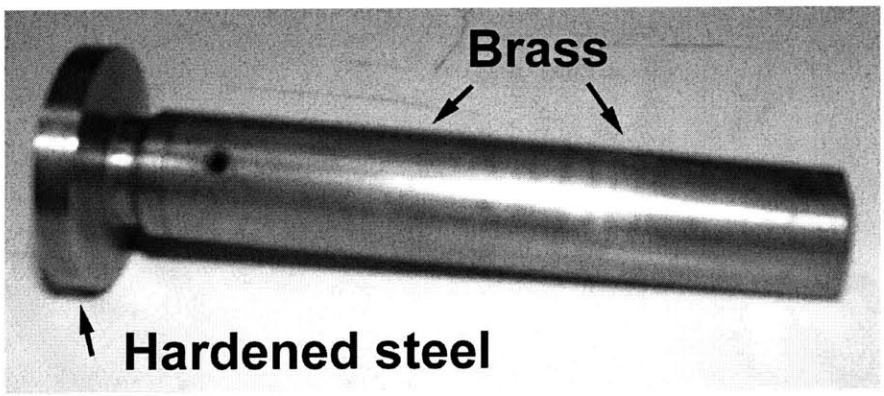

Figure A1.2: Photograph of the new intake lifter

Lift	Maximum pushrod force
6.2 mm	217.9 lbf
5 mm	160.4 lbf
4 mm	118.1 lbf
3 mm	81.0 lbf
2 mm	49.0 lbf

Table A1.1: Maximum pushrod force for each lift

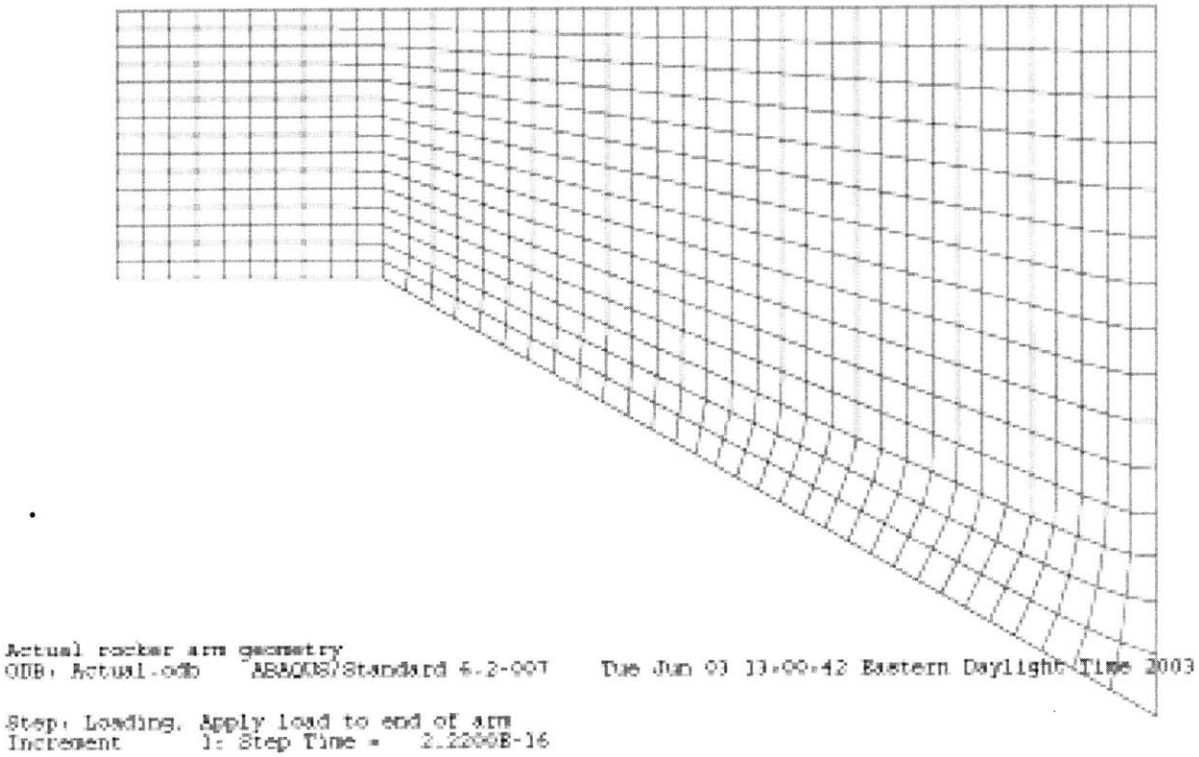

Figure A1.3: ABAQUS screen capture of actual rocker arm geometry with mesh (undeformed).

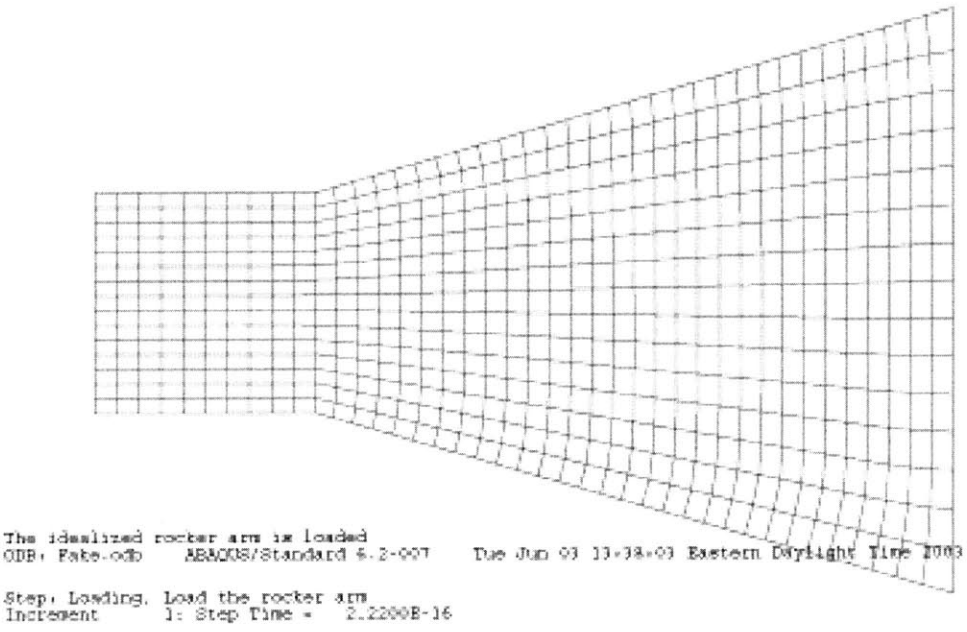

Figure A1.4: ABAQUS screen capture of pseudo rocker arm geometry with mesh (undeformed).

		Maximum Mises' equivalent stress
Top of arm	Actual geometry	6.5 ksi
	Pseudo geometry	6.3 ksi
Bottom of arm	Actual geometry	7.4 ksi
	Pseudo geometry	6.5 ksi

Table A1.2: Summary of maximum Mises' equivalent stresses for actual and pseudo geometry

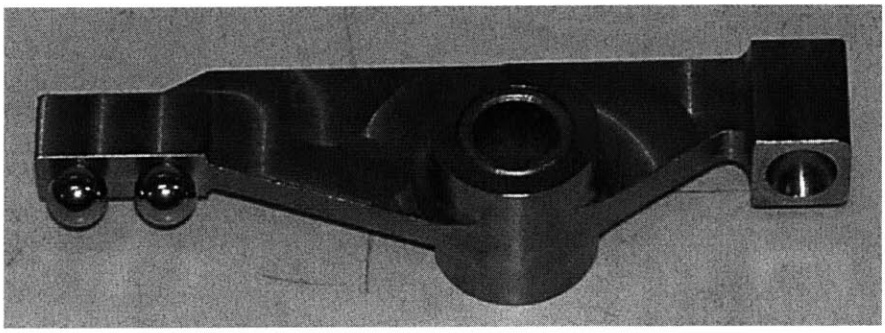

Figure A1.3: Photograph of the 4 and 5 mm rocker arm

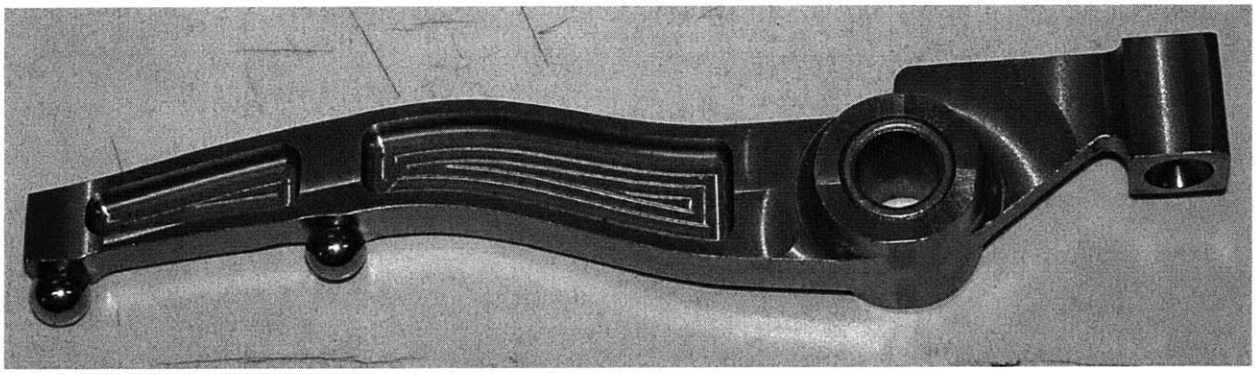

Figure A1.3: Photograph of the 2 and 3 mm rocker arm